MICROCOPY RESOLUTION TEST CHART

NATIONAL BUREAU OF STANDARDS-1963

AFOSR-TR-77-1313

NONDESTRUCTIVE EVALUATION OF METAL FATIGUE

by
F. N. Kusenberger
G. A. Matzkanin
J. R. Barton
P. H. Francis
J. Lankford
C. M. Teller

FEB 2 1978
F

FINAL SCIENTIFIC REPORT
SwRI Project No. 15-4163

SOUTHWEST RESEARCH INSTITUTE
SAN ANTONIO   CORPUS CHRISTI   HOUSTON

"Qualified requestors may obtain additional copies from the Defense Documentation Center, all others should apply to the National Technical Information Service."

CONDITIONS OF REPRODUCTION

REPORT DOCUMENTATION PAGE		READ INSTRUCTIONS BEFORE COMPLETING FORM
1. REPORT NUMBER AFOSR-TR-77-1313	2. GOVT ACCESSION NO.	3. RECIPIENT'S CATALOG NUMBER
4. TITLE *(and Subtitle)* NONDESTRUCTIVE EVALUATION OF METAL FATIGUE,		5. TYPE OF REPORT & PERIOD COVERED Final scientific rept. Jan 1975 - Sept 1977 6. PERFORMING ORG. REPORT NUMBER SwRI Project 15-4163
7. AUTHOR(s) F. N. Kusenberger, P. H. Francis G. A. Matzkanin, J. Lankford J. R. Barton, C. M. Teller		8. CONTRACT OR GRANT NUMBER(s) F44620-75-C-0042
9. PERFORMING ORGANIZATION NAME AND ADDRESSES Southwest Research Institute 6220 Culebra Rd., P.O. Drawer 28510 San Antonio, Texas 78284		10. PROGRAM ELEMENT, PROJECT, TASK AREA & WORK UNIT NUMBERS 2307 9782 61102F
11. CONTROLLING OFFICE NAME AND ADDRESS Air Force Office of Scientific Research/NA Bldg 410 Bolling Air Force Base, DC. 20332		12. REPORT DATE Nov 1977 13. NUMBER OF PAGES 66 24 P.
14. MONITORING AGENCY NAME & ADDRESS *(if different from Controlling Office)*		15. SECURITY CLASS. *(of this report)* Unclassified 15a. DECLASSIFICATION/DOWNGRADING SCHEDULE

16. DISTRIBUTION STATEMENT *(of this Report)*

Approved for public release; distribution unlimited

17. DISTRIBUTION STATEMENT *(of the abstract entered in Block 20, if different from Report)*

18. SUPPLEMENTARY NOTES

19. KEY WORDS *(Continue on reverse side if necessary and identify by block number)*

Nondestructive Testing   Fracture Mechanics
Magnetic Leakage Field   Magnetic Inspection
Fatigue Tests

20. ABSTRACT *(Continue on reverse side if necessary and identify by block number)*

Nondestructive evaluation investigations have been conducted of surface entering fatigue cracks in rod-shaped tensile specimens of AISI 4340 and HY 180 steels. To alleviate the need for constant manual monitoring of the fatigue machine for specimens requiring many stress cycles, an automated monitoring capability based on detection of fatigue cracks by surface wave ultrasonics was fabricated. Fatigue cracks up ...

DD FORM 1473   EDITION OF 1 NOV 65 IS OBSOLETE
1 JAN 73

328 200 JOB

20.

to 0.050-in.-long were studied using magnetic perturbation, surface wave ultrasonics and Barkhausen noise analysis. Results showed the minimum detectable flaw size in HY 180 steel using surface wave ultrasonics to be 2 to 3 times the minimum size detectable in AISI 4340 steel. Also an applied load is necessary to ultrasonically detect fatigue cracks as long as 0.030-in. in HY 180. Extensive magnetic perturbation measurements were made on an AISI 4340 steel specimen cycled near yield. Attempts to interpret the behavior of the signal amplitude with applied static stress in terms of available closure models were not entirely successful. Indications are that the effect of plastic deformation in the vicinity of the crack on the magnetic perturbation signal must be taken into account. The magnetic perturbation signal peak separation was found to depend on crack length in a nonlinear fashion and to be affected by the plastic zones at the crack tips. Other investigations conducted included fractography to study the fracture surfaces and fatigue crack initiation sites in AISI 4340 and HY 180, microhardness measurements of plastic zones, and extension of an analytical model for calculation of magnetic leakage fields from surface entering fatigue cracks.

SOUTHWEST RESEARCH INSTITUTE
Post Office Drawer 28510, 6220 Culebra Road
San Antonio, Texas 78284

NONDESTRUCTIVE EVALUATION OF METAL FATIGUE

by

F. N. Kusenberger
G. A. Matzkanin
J. R. Barton
P. H. Francis
J. Lankford
C. M. Teller

FINAL SCIENTIFIC REPORT
SwRI Project No. 15-4163

Prepared for
Air Force Office of Scientific Research
Directorate of Aerospace Sciences
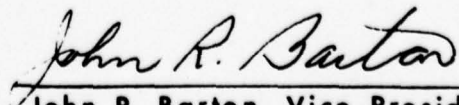**Contract F44620-75-C-0042**
Project No. 9782-05

November 1977

Research Sponsored by Air Force Office of Scientific Research
Directorate of Aerospace Sciences, United States Air Force

"Approved for public release; distribution unlimited"

Approved:

John R. Barton

John R. Barton, Vice President
Instrumentation Research Division

ABSTRACT

Nondestructive evaluation investigations have been conducted of surface entering fatigue cracks in rod-shaped tensile specimens of AISI 4340 and HY 180 steels. To alleviate the need for constant manual monitoring of the fatigue machine for specimens requiring many stress cycles, an automated monitoring capability based on detection of fatigue cracks by surface wave ultrasonics was fabricated. Fatigue cracks up to 0.050-in.-long were studied using magnetic perturbation, surface wave ultrasonics and Barkhausen noise analysis. Results showed the minimum detectable flaw size in HY 180 steel using surface wave ultrasonics to be 2 to 3 times the minimum size detectable in AISI 4340 steel. Also an applied load is necessary to ultrasonically detect fatigue cracks as long as 0.030-in. in HY 180. Extensive magnetic perturbation measurements were made on an AISI 4340 steel specimen cycled near yield. Attempts to interpret the behavior of the signal amplitude with applied static stress in terms of available closure models were not entirely successful. Indications are that the effect of plastic deformation in the vicinity of the crack on the magnetic perturbation signal must be taken into account. The magnetic perturbation signal peak separation was found to depend on crack length in a nonlinear fashion and to be affected by the plastic zones at the crack tips. Other investigations conducted included fractography to study the fracture surfaces and fatigue crack initiation sites in AISI 4340 and HY 180, microhardness measurements of plastic zones, and extension of an analytical model for calculation of magnetic leakage fields from surface entering fatigue cracks.

TABLE OF CONTENTS

LIST OF ILLUSTRATIONS

LIST OF ILLUSTRATIONS (Cont'd)

I.   INTRODUCTION AND SUMMARY

As is well known, materials used in aerospace vehicles and components are never perfect, but contain varying numbers and distributions of inherent flaws as well as fabrication defects. Additionally, operational service introduces other defects such as fatigue cracks and also detrimental residual stress distributions. The occurrence of these defects is a critical factor controlling the design and life cycle cost of modern aerospace structures. Thus, it is important to understand these defects and stresses and how they influence material properties and performance in order to assess structural airframe and engine subsystem integrity. Basic to a more complete understanding of the influence of material defects are methods and techniques for nondestructive evaluation (NDE). What is needed are quantitative NDE capabilities to characterize defects in terms of type, location, number distribution, size, shape, and associated residual stresses. Such knowledge is necessary in modern aerospace design philosophy whereby fracture mechanics analysis is used to configure a safe structure even though flaws are present.

In recognition of the importance of obtaining quantitative information on defects, emphasis of the fatigue evaluation program at Southwest Research Institute has been on investigating NDE techniques for quantitative characterization of fatigue crack parameters to enable an assessment of the crack criticality by fracture mechanics analysis. The NDE methods used have been magnetic perturbation, surface wave ultrasonics, Barkhausen noise analysis, electric current injection, and AC four-contact electric probe. The general methodology consists of fatigue cycling carefully prepared notch-free, rod-type, tensile specimens and correlating directly measured and/or calculated crack parameters, such as: crack length, crack opening displacement, crack interface area, crack depth, and the residual stress field and plastic deformation in the immediate vicinity of the crack with results of the NDE investigations. Crack parameters are determined directly by optical microscopy, scanning electron microscope examination of plastic replicas, fractography and microhardness measurements. In addition to experimental investigations, analytical efforts have been directed toward developing mathematical models functionally relating the NDE signatures with crack characteristics.

The contract period dovered by this Final Report extends from 1 January 1975 through 30 September 1977; however, the first two years of this period are covered by Interim Reports issued in March 1976 and February 1977, respectively. Therefore, this report will emphasize results ofbtained during the latter nine months of the contract period, and will only summarize results from the two Interim Reports. One correction pertaining

to the February 1977 Interim Report should be noted. The material described in that report as AF 1410, was in fact HY 180 steel. An errata is included as Appendix A in this report.

Magnetic perturbation and surface wave ultrasonic measurements were performed on steel specimens of AISI 4340 and HY 180. Since the HY 180 is produced by vacuum induction melting/vacuum arc remelting (VIM/VAR), it contains very few metallurgical inclusions and thus, a large number of stress cycles are needed to generate fatigue cracks in smooth specimens. To alleviate the need for constant manual monitoring of the specimen during stress cycling, an electronic system was designed and installed to automatically and continuously monitor six ultrasonic surface wave transducers mounted on the specimen.

Crack lengths up to 0.050-in.-long were grown in AISI 4340 and HY 180 specimens. Comparison of surface wave ultrasonics and magnetic perturbation NDE responses showed significant differences between the two materials. The ultrasonic background noise was found to be somewhat greater in HY 180 so that the minimal detectable flaw size using surface wave ultrasonics is approximately three times the size flaw detectable in AISI 4340. Investigation of the microstructure of these two materials revealed characteristics which may account for the greater background noise in HY 180. For both materials, the magnetic perturbation signal is composed of two components, a principal component and a smaller, broader, secondary "satellite" component of opposite polarity (see Figure 2). The satellite signatures were found to be much more prominent in HY 180 than in AISI 4340 which may aid fatigue crack detection. Also, magnetic perturbation results on HY 180 indicate that earliest crack detection in this material is obtained under high magnetic field conditions, contrary to the case for AISI 4340, and significant enhancement of detection is obtained by applying load. Since much Air Force inspection of magnetic materials is performed using methods such as magnetic particles, the different magnetic characteristics observed between HY 180 and AISI 4340 steel could have important implications for guiding establishment of future inspection criteria.

Investigation showed that once a crack is opened by applied load, the magnetic perturbation signal amplitude at the center of the crack is linearly related to the crack opening displacement (COD). The nonlinear changes in signal amplitude that are observed at low loads may be interpreted in terms of signal contributions from the inclusion, and crack closure effects. Results obtained from an AISI 4340 steel specimen (S5) cycled at a peak stress level near yield showed that the magnetic perturbation signal amplitude varied similarly with stress for all scan tracks along the crack interface. A closure model for center and edge notched specimens indicates that the center of the crack should open first under

load, thus, the magnetic perturbation results imply that the closure effect may be small for the specimen investigated. Since the specimen investigated was cycled at a high stress level, it is likely that the signals will also be influenced by the heavily deformed plastic zones around the crack. Lack of an adequate analytical model for the effect of magneto-mechanical interactions produced by plastic deformation on magnetic perturbation signals precludes an analysis of the influence of the plastic zones at this time.

Evidence was obtained indicating that the magnetic perturbation signal peak separation may be influenced by plastic zones associated with fatigue cracks. This conclusion is based upon observations that

(1)   the peak separation is less for scans near the crack center than for those near the tips where the stress zones are larger, and

(2)   the peak separation near the crack tip varies considerably with crack length.

Details of the summary results presented above are presented in Section II of this report along with supporting experimental evidence. Additional background information on fatigue crack detection and characterization may be found in earlier AFOSR Final Reports. [1, 2]

The promising results obtained to date indicate the importance of these continuing efforts for developing improved NDE methods for quantitative characterization of small flaws and fatigue cracks. Ability to characterize fatigue cracks quantitatively in conjunction with fracture mechanics, should provide a scientific basis for assessing the criticality of detected cracks. This would be of great importance to the Air Force in relation to design criteria for structural configurations as well as an improved basis for maintenance decisions.

II. EXPERIMENTAL PROCEDURES

A. General

The basic experimental procedure consisted of initiating and propagating fatigue cracks by cycling the specimens at selected values of maximum uniaxial tensile stress (stress ratio R=0). For fatigue cycling, a Double Unit Direct Stress Fatigue Testing Machine manufactured by the Budd Company was used. During fatigue cycling the specimens were continuously monitored using a pulse echo ultrasonic method and six 10 MHz surface wave transducers bonded to machined flats on the fatigue test specimens. After initiation of a fatigue crack was noted in the ultrasonic response, the largest crack (in the case of more than one crack), determined by measuring surface length with an optical microscope, was chosen for further investigation. At various stages of crack growth, the fatigue machine was stopped, and both direct laboratory measurements and NDE measurements of crack parameters were made. To provide information on the influence of applied stress, measurements were made over a range of applied static loads from zero to the peak tensile load applied during fatigue cycling. Where possible, crack parameters were obtained without removing the specimen from the fatigue machine. Direct crack length measurements were made with an optical microscope, and surface photomicrography (approximately 100X magnification) was performed to record the surface crack geometry. In a few cases, plastic replicas were made for determination of the crack opening displacement using a scanning electron microscope (SEM).

To provide information on crack interface area and morphology, macroscopic fractography was conducted on one AISI 4340 and one HY 180 steel specimen each of which had been stress cycled at 180 ksi. In addition, information on the plastic zone size at the fatigue crack tip was obtained from microhardness measurements made on an AISI 4340 steel specimen containing a 0.050-in.-long surface entering crack. The center portion of the specimen was sectioned and mounted so that polishing could be carried out approximately normal to the crack plane. Polished sections were obtained at depth of 0.001-in. to 0.002-in., 0.002-in. to 0.003-in., and approximately 0.010-in. At each depth a diamond pyramid under a load of 0.002 lb. was used to obtain the microhardness profile along traces both normal and parallel to the crack plane.

B. Apparatus

Information regarding details of the fatigue machine and NDE instrumentation has been reported previously.[3] A brief discussion of the various NDE methods used in these investigations is given in Appendix B.

Because HY 180 steel is VIM/VAR processed, and thus, contains very few metallurgical inclusions, it was anticipated that a large number of stress cycles would be necessary to generate fatigue cracks. Therefore, an automatic monitoring capability for the stress cycling machine was designed and installed to alleviate the need for constant manual monitoring of the specimen. A block diagram of the automatic monitoring system for the fatigue machine is shown in Figure 1. Ultrasonic echoes reflecting from fatigue cracks and exceeding a preset threshold level send an alarm signal to the microcomputer. Recognition of fatigue crack initiation by the microcomputer results in a command to shut down the fatigue machine. Pertinent information such as cycle count and alarm and the transducer initiating the alarm is printed by a teletype terminal. The system can be expanded for processing of ultrasonic signals, or other information, such as magnetic perturbation signals and Barkhausen noise signals, by integration with either a Tektronix 4051 Graphic Computing System or a Hewlett-Packard 2100 Minicomputer available for this purpose.

C.   Specimens

The specimens used in the experiments were polished, rod-type specimens of AISI 4340 steel and HY 180 steel. Six flats were machined near one end of the specimens for bonding of the ultrasonic transducers. After heat treatment, machining, and polishing, measurements showed the AISI 4340 and the HY 180 steel specimens to have an average 0.2% offset tensile yield strength of 183 ksi and 183.6 ksi, respectively. Details of the specimen preparation, heat treatment schedule, and the average mechanical properties are given in Appendix C.

Experimental procedures specific to the various NDE methods are briefly described in the next section in conjunction with discussion of experimental results.
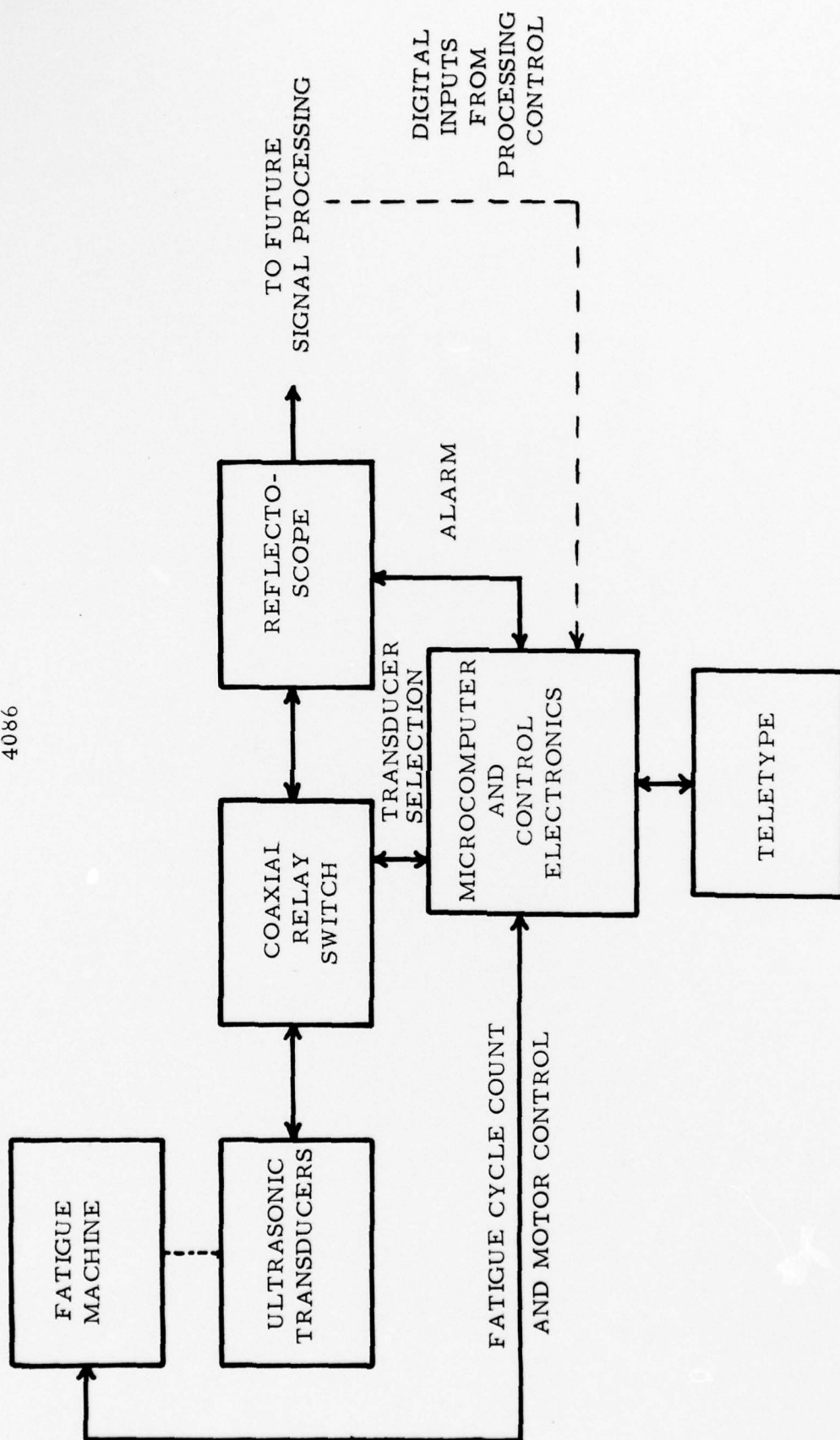
FIGURE 1. BLOCK DIAGRAM OF AUTOMATED CONTROL SYSTEM FOR STRESS-CYCLING MACHINE.

6

4086

III. RESULTS AND DISCUSSION

A. Analysis of Magnetic Perturbation Results

Magnetic perturbation signals were obtained with a small Hall effect probe (0.001-in. x 0.004-in.). The probe was mechanically moved on a precise path along the specimen axis (perpendicular to the crack interface) by means of a scanning mechanism. The width of the scan track interrogated by the probe is not precisely known, but it is probably no more than 0.002-in. In general, prior to stress cycling, the specimens were surveyed with the magnetic perturbation instrumentation. The specimens were then stress cycled in tension to initiate fatigue cracks. The fatigue machine was stopped at various stages of crack growth and for each crack length magnetic perturbation measurements were made at different values of applied static stress up to the maximum cyclic stress. Data were obtained with the specimen magnetized nearly to saturation using a magnetizing current of 6.0 amp (hereafter referred to as the "high field" or HF condition) and also at a lower magnetizing current of 0.8 ampere ("low field" or LF condition). For each crack length and applied stress, magnetic perturbation signatures were obtained from a number of adjacent tracks perpendicular to the crack interface. As reported previously[2], the signature usually consists of two components as shown in Figure 2. The signal parameters extracted for analysis were:

(1)   principal signal amplitude
(2)   satellite signal amplitude
(3)   principal signal peak separation
(4)   satellite signal peak separation

All of the recorded data were reduced and plotted using a Tektronix 4051 Graphic Computing System.

1. Comparison Between HY 180 and AISI 4340 Steel Specimens

Figure 3 presents characteristic magnetic perturbation signatures obtained at several locations along a 0.025-in.-long fatigue crack in AISI 4340 steel (Specimen S30) and also along a 0.026-in.-long fatigue crack in HY180 steel (Specimen H1). The crack shown in the illustration was in the AISI 4340 specimen and the signatures shown beneath the crack were obtained from this specimen. The signatures above the crack photograph were obtained from the HY 180 specimen. Examination of these and similar results on cracks of other lengths shows that there are significant differences in magnetic perturbation signature characteristics obtained from
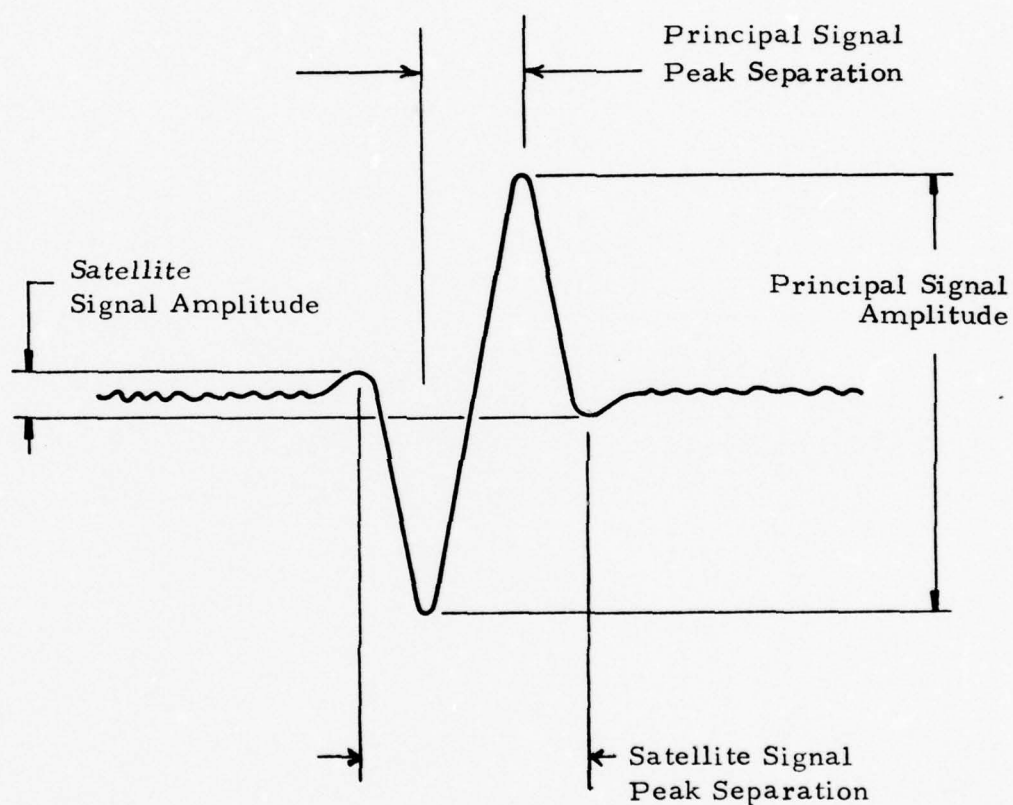
3059 a

FIGURE 2. CHARACTERISTIC MAGNETIC SIGNATURE ASSOCIATED
WITH A SURFACE CRACK

4382

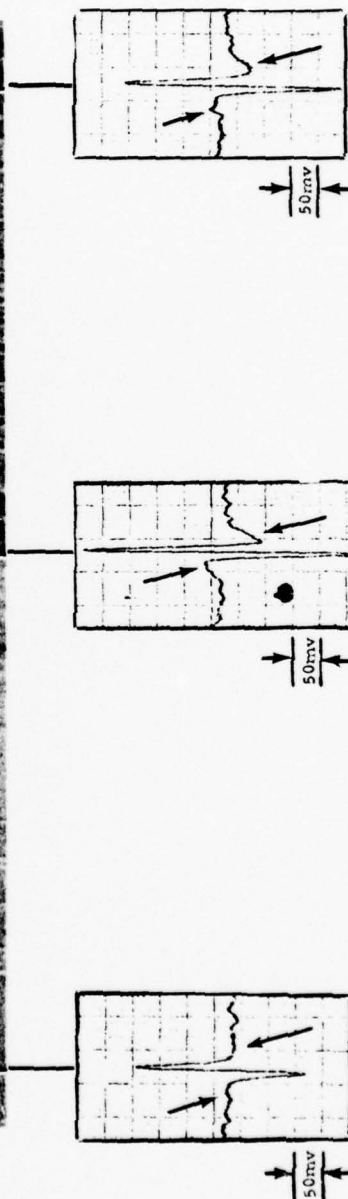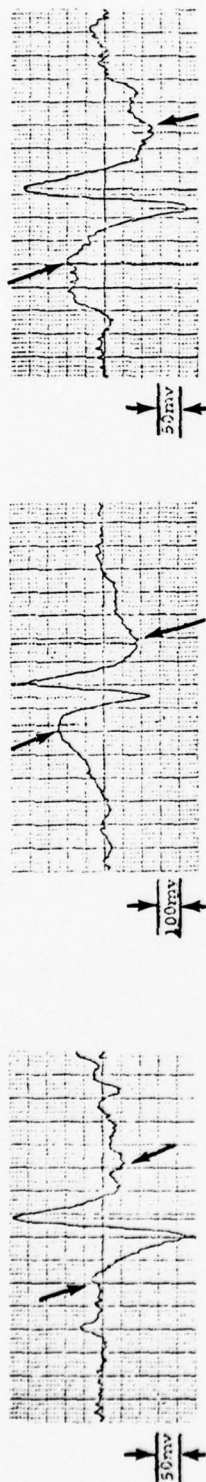HY-180 (Specimen H-1, High Field, Stress = 170 ksi)

Specimen S30
High Field
Stress = 125 ksi

0.005 in.

AISI 4340

FIGURE 3. CHARACTERISTIC MAGNETIC PERTURBATION SIGNATURES

9

similar length cracks in HY 180 and AISI 4340. For example, as can
be seen, the satellite signatures are much more prominent in HY 180
than in AISI 4340 steel. Previous results obtained from fatigue cracks
and artificially produced geometric discontinuities, such as electric-
discharge machined slots, in AISI 4340 steel, have indicated that the
satellite signatures may be associated with elastic and plastic strains[4].
Since the magneto-elastic response of HY 180 may be considerably
different from AISI 4340, the prominent satellite signatures in HY 180
could be an aid to fatigue crack detection.

Extension of the crack in Specimen H1 resulted in
a large increase in amplitude of the principal component but a very small
increase in the satellite amplitude. This is illustrated in Figure 4 which
shows selected signatures and a photograph obtained after the crack in
Specimen H1 was propagated to a length of 0.050-in. For the signature
at the center of the crack, the satellite amplitude has increased only
slightly (300mV) compared with the satellite (240mV) when the crack was
only 0.026-in. long (see Figure 3). By contrast, the principal component
has increased dramatically; 2075mV (Figure 4) compared to 640mV
(Figure 3).

Prior research has confirmed that earliest detection
of fatigue cracks in AISI 4340 steel is obtained under relatively low mag-
netic field conditions[2]; however, the results on HY 180 indicate that
earliest crack detection in this material is obtained under high flux con-
ditions, and significant enhancement of detection is obtained by applying
load. If these preliminary results are confirmed by more extensive
experiments, they could be of significance in providing guidance for the
inspection of certain magnetic materials. For example, relatively low
magnetic field conditions are currently used in the inspection of many
parts using the magnetic particle inspection method. The results obtained
here indicate that use of low field magnetizing conditions for magnetic
particle inspection of HY 180 components would result in less than
optimum capability for detecting fatigue cracks.

2.   Relationship of Magnetic Perturbation Signal to
       Crack Opening Displacement and Crack Length

Representative results for the variation of the magnetic
perturbation signal amplitude along the crack interface are shown in
Figure 5. These results are for a 0.052-in.-long fatigue crack in AISI 4340
steel (Specimen S5) with an applied static stress of 180 ksi. In general,
the satellite component is observed for only a short distance beyond the
crack tip, whereas, the principal component is observable well beyond the
crack tips. Previous investigations have explored the relationship between

4383

0.010 in.

Specimen H-1
High Field
Stress = 170 ksi

250mv

250mv

250mv
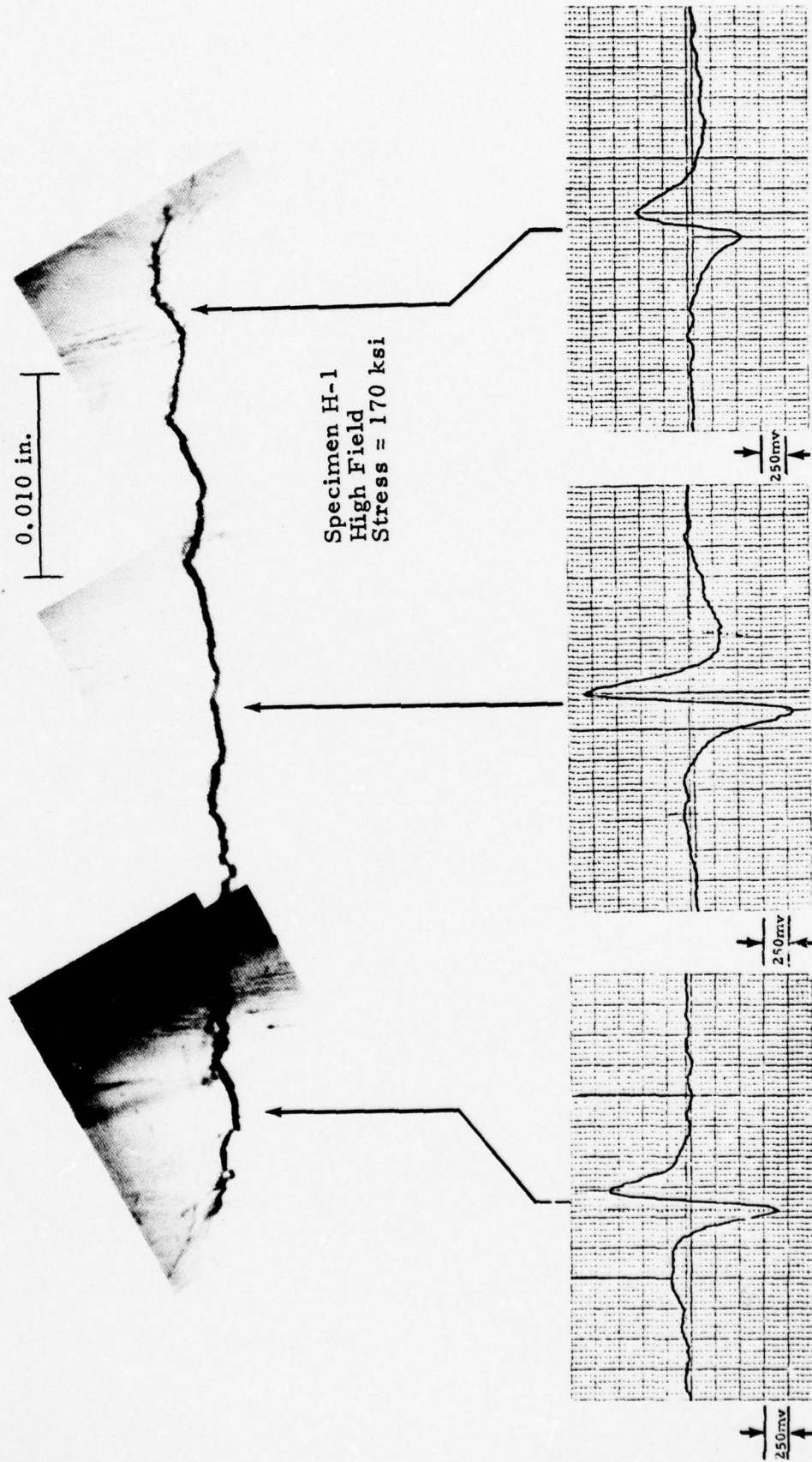
FIGURE 4. FATIGUE CRACK (0.050-in.) IN HY 180 STEEL SPECIMEN WITH ASSOCIATED MAGNETIC PERTURBATION SIGNATURES

4091

7/9/76   SPECIMEN:S-5   MATERIAL:4340 STEEL
CRACK LENGTH:0.052"   NO. CYCLES:?900   COMMENTS:CRACK "B"
LOAD:FL   FL=180KSI   FIELD:HF

+ PRIN.

▲ SAT.

CRACK

AMPLITUDE (MV)

2200 2000 1800 1600 1400 1200 1000 800 600 400 200 0 -200 -400

250 260 270 280 290 300 310

SCAN TRACK LOCATION (DEG) (1 DEG ≅ 0.002 in.)

FIGURE 5.   MAGNETIC PERTURBATION SIGNAL AMPLITUDE VERSUS
LOCATION ALONG A FATIGUE CRACK.

the magnetic perturbation signal amplitude and the COD for various crack lengths in several different specimens. [4] It was found that a linear relationship exists between the magnetic perturbation signal principal component amplitude and the COD at the center of the crack ($COD/_{max}$), and that for crack lengths from 0.030-in. to 0.050-in. this relationship is approximately independent of crack length.

An example of the relationship between the $COD/_{max}$ and the amplitudes of both the principal and satellite components is shown in Figure 6 for AISI 4340 steel (Specimen S29). The data plotted are the magnetic perturbation signal amplitude (scan track over crack center; HF condition) versus applied static tensile stress σ_∞ expressed as a fraction of the peak cyclic stress σ_p. Within the elastic region the crack length remains unchanged as static load is applied to a specimen containing a fatigue crack of a certain length. Since application of a saturating magnetic field minimizes the influence of magnetostrictive effects (i.e., permeability variation), these curves illustrate mainly the influence of crack opening produced by the applied load on the magnetic perturbation signals. The same signal data replotted in terms of $COD/_{max}$ as determined by SEM measurements of plastic replicas are presented in Figure 7. As shown, once $COD/_{max}$ equals approximately 50×10^{-6} inch, the magnetic perturbation signal amplitude of both the principal and satellite components is linearly dependent on crack opening. Prior to this threshold value, the amplitude of the principa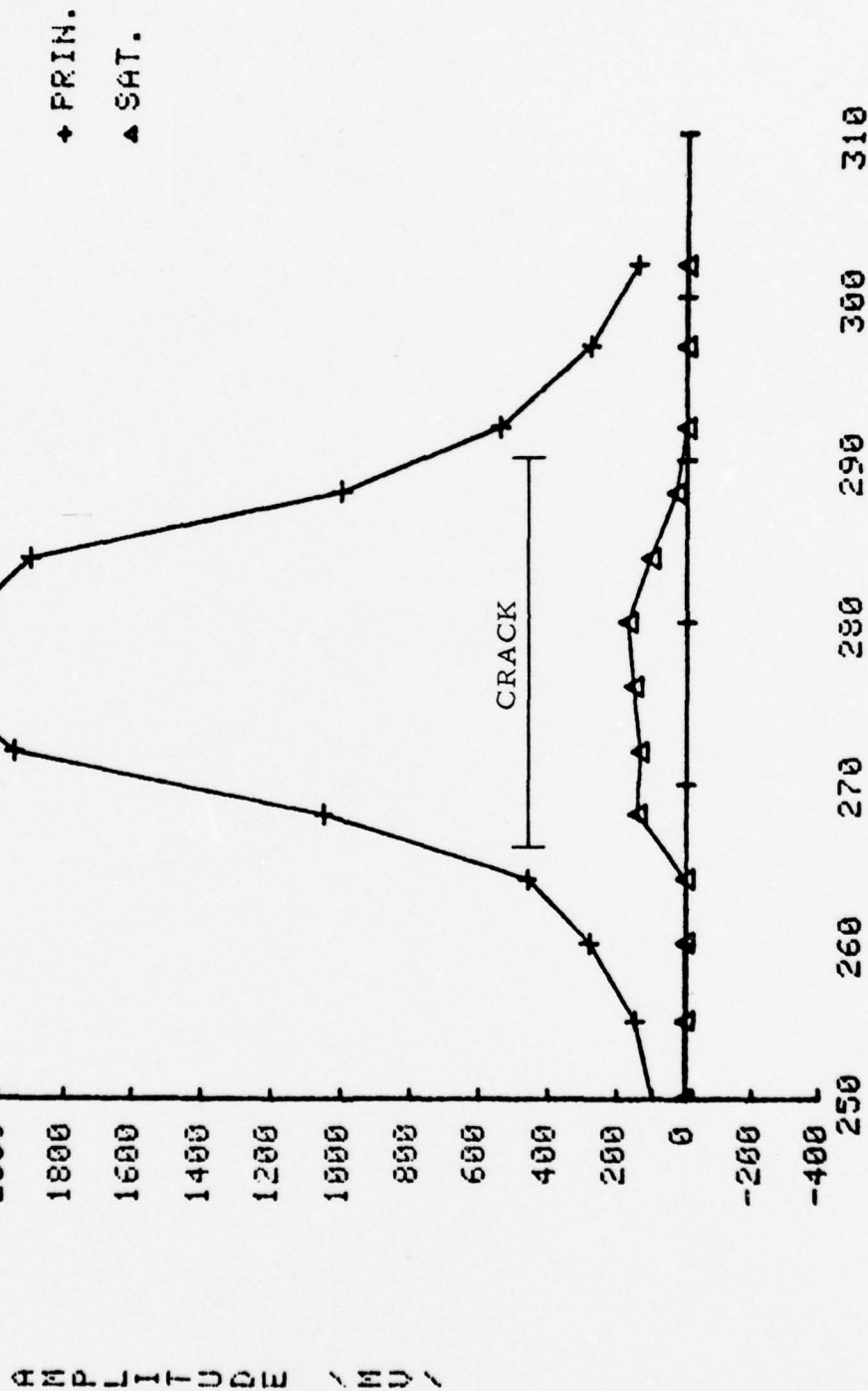l component changes only slightly and the satellite component is not detectable (satellite components have been observed on other specimens at small COD levels, however). Note also in Figure 7 that the linear relationship between the magnetic perturbation signal amplitude and $COD/_{max}$ extrapolates to zero for this specimen. These results may be attributable to closure stresses which prevent the crack from opening until the applied stress becomes great enough. However, as discussed in the next section, further data on additional specimens fails to entirely support this explanation. Calculations of the magnetic leakage field caused by a void have shown that the magnetic perturbation signal amplitude is linearly dependent on the air volume of the void. [5] Thus, the results obtained here suggest that the volume between the crack interfaces is a linear function of $COD/_{max}$.

3.   Crack Closure Considerations

Crack closure refers to the phenomenon noted by Elber and others in center-notched and edge-notched specimens, that once a crack has experienced at least one complete load cycle the crack region near the tip will remain closed for a certain amount of tensile load upon reloading. [6] It is believed that closure of the crack interface at the crack tips under no-load is caused by residual compression stresses in the plastic enclaves. Since these compression stresses prevent immediate opening of the crack
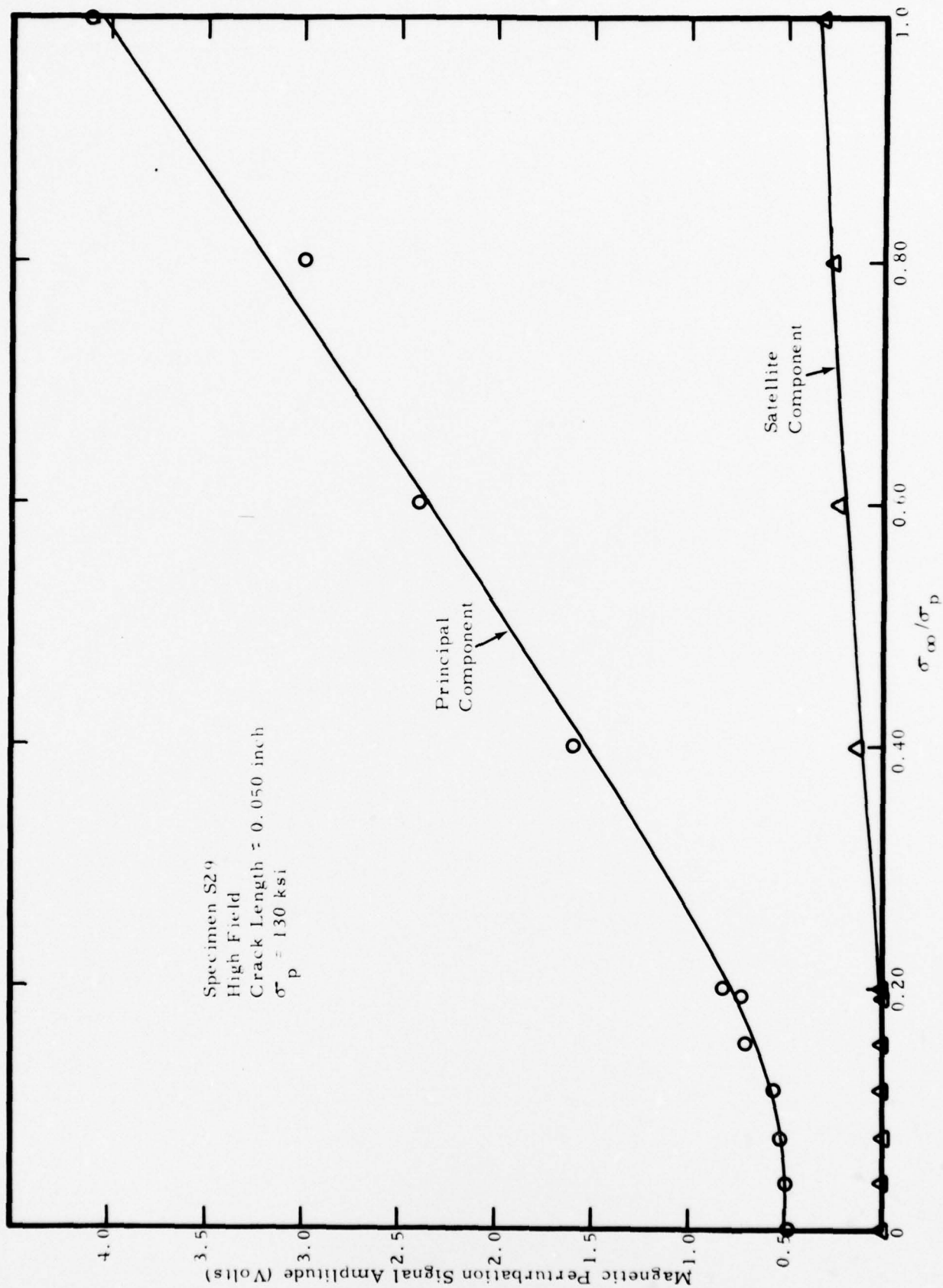
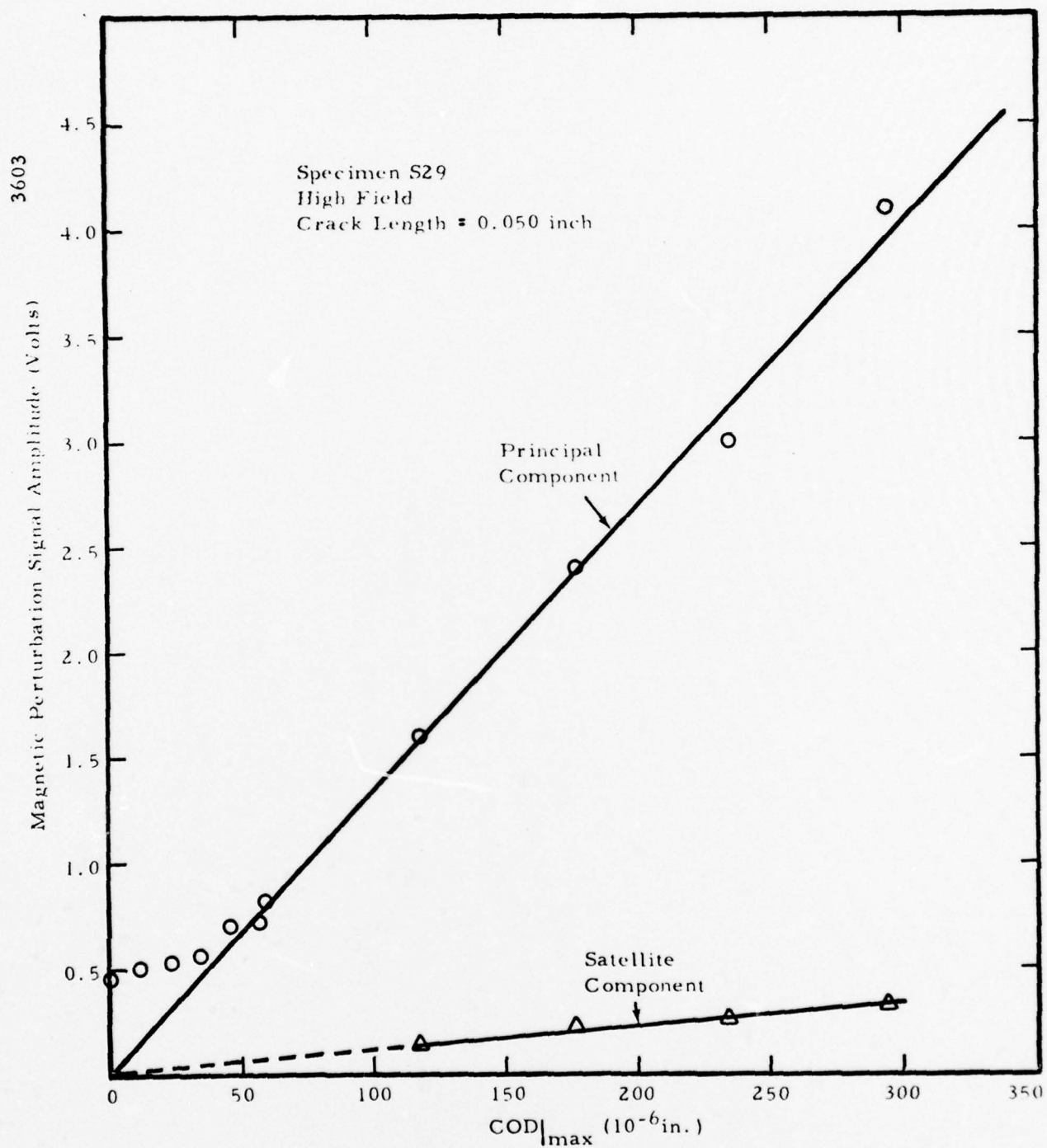FIGURE 6. MAGNETIC PERTURBATION SIGNAL AMPLITUDE VERSUS APPLIED STRESS

14

FIGURE 7. MAGNETIC PERTURBATION SIGNAL AMPLITUDE VERSUS COD$|_{max}$

as load is applied, it is plausible that this mechanism might partially amount for the nonlinear change of the magnetic perturbation signal amplitude with load found at low stress levels. In addition to crack closure, however, the inclusion is also expected to contribute to the magnetic perturbation signal at low loads.

As discussed in the previous section, the magnetic perturbation signal amplitude changes slowly at first as the load is increased and then varies linearly with $COD/_{max}$ beyond a certain load level (see Figures 6 and 7). These results are consistent with an interpretation in terms of crack closure. However, the general pattern of magnetic perturbation signal amplitude change with load at different positions along the crack interface in a specimen cycled at a high stress level is not consistent with the usual conception of a closure model, at least for center and edge notched specimens, whereby the crack is closed by a pattern of residual stresses and strains at the crack tip. Since the center of the crack is farthest from the crack tips, it would be expected to open first under load before other positions on the crack interface open. It would not, therefore, be expected that all positions on the crack interface would be open at the same value of applied load unless the closure effect was very small. In Figure 8 are plotted the magnetic perturbation signal amplitude versus applied stress for a 0.030-in.-long crack in *Specimen S5, cycled at at stress level near yield, for a number of probe* scans along the crack interface. In these plots the scan track locations is designated in terms of circumferential degrees around the specimen. A one-degree increment corresponds to 2.2×10^{-3} inch. The particular tracks associated with the crack center and crack tips are indicated on the figure. As can be seen, in most cases, the magnetic perturbation signal amplitude behaves similarly with stress for all scan tracks along the crack interface, thus implying a small closure effect according to the model discussed above. This is in agreement with results of acoustic investigations which show the closure effect to be small for part-through cracks 0.103-in.-long in AISI 4340 steel.[7] In addition, if the entire crack interface were closed under no-load then the magnetic perturbation signal amplitudes for the various scan tracks would be expected to all have approximately the same value at zero load. Experimentally, the magnetic perturbation signal amplitude at no-load varies considerably along the crack interface implying that some crack void may still exist at zero load possibly beneath a surface closure. Such a result has been reported by others for through cracks.[8]

It should be emphasized that the analysis presented here is based upon data obtained on a specimen cycled at a stress level near yield. Because of the high stress level involved, it is expected that magnetic perturbation signals will also be influenced by the heavily deformed plastic zones around the crack. Similar experiments on specimens

4619

SPECIMEN: S-5   NO. CYCLES: 8800
CRACK LENGTH: 8.03 IN.   MATERIAL: 4340 STEEL
6/24/77   FIELD: HF   CRACK B

Peak Stress: 180 ksi

Crack Center – 278°

Crack Tips – {271°
             {285°

276°
278°
280°
274°

272°
282°

270°

268°

AMPLITUDE (MV)

STRESS (KSI)

20 40 60 80 100 120 140 160

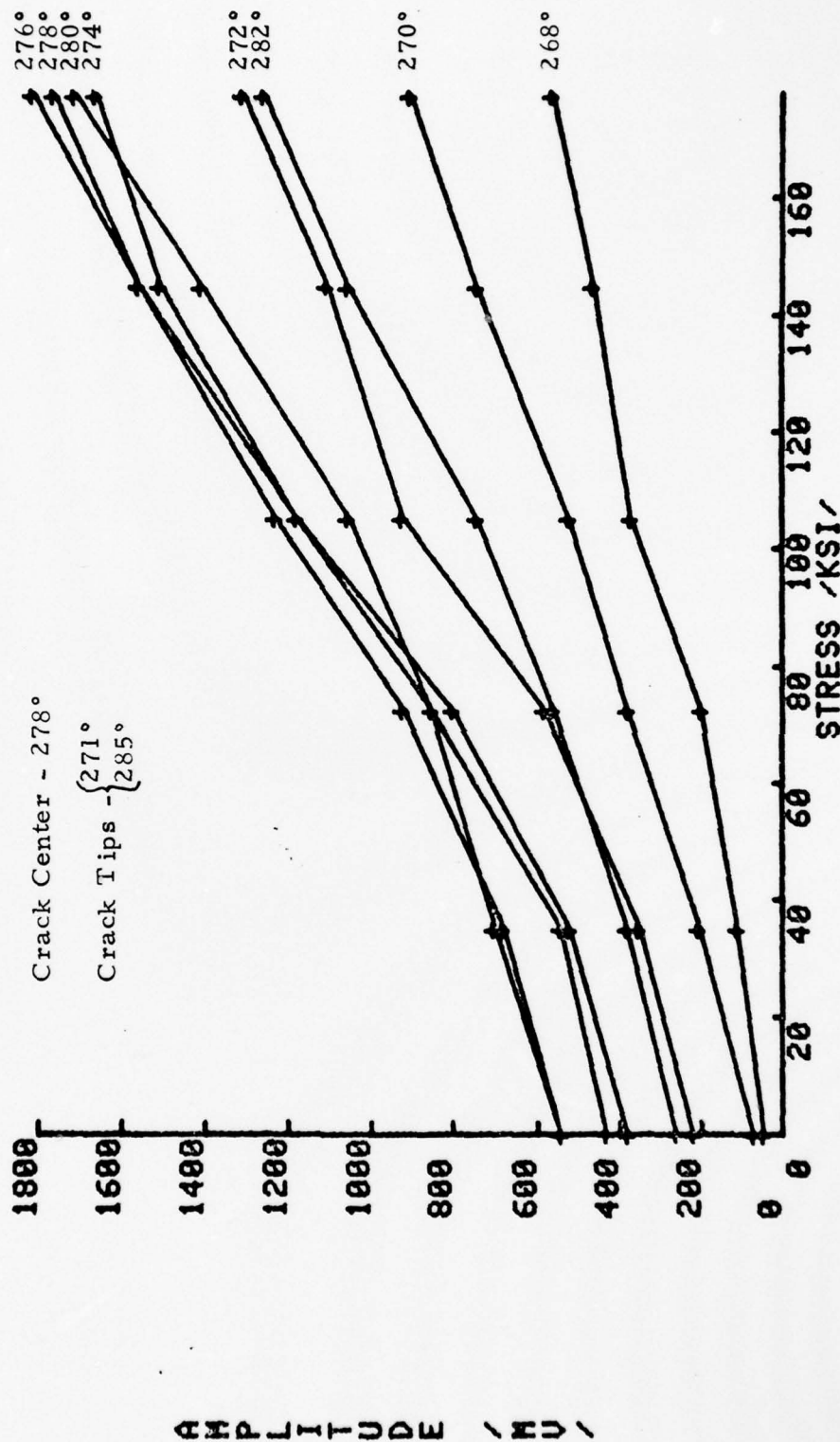0 200 400 600 800 1000 1200 1400 1600 1800

FIGURE 8.   PRINCIPAL SIGNAL PEAK AMPLITUDE VERSUS STRESS FOR VARIOUS
            SCAN TRACKS ALONG THE CRACK INTERFACE

cycled at other stress levels are necessary to clarify the influence of closure effects. Development of analytical models taking into account changes in the magnetic characteristics associated with magneto-mechanical interactions will help provide a more complete explanation for the behavior of magnetic perturbation signals in the vicinity of fatigue cracks.

4.   Analysis of Magnetic Perturbation Signal Peak
        Separation

        Measurements were made of the separation between the peaks of the magnetic perturbation signal (refer to Figure 2) in order to explore the possible relationship between this parameter and the crack geometry. In general, the peak separation of both the principal and satellite components is less at the interior regions of the crack than at the tips, as shown in Figure 9 for Specimen S5. These results are observed consistently for all crack lengths and applied loads investigated. Although no detailed explanation has been developed at this time, these results suggest that peak separation may be related to stressed zones around fatigue cracks. This hypothesis is supported by the observation that for low magnetic fields the variation in signal peak separation from interior regions of the crack to the tip is greater than for the high field case (see Figure 9).

        As is well documented by previous experiments on non-magnetic inclusions in ferromagnetic alloys, there is an approximately linear relationship between magnetic perturbation peak separation and distance from the surface to the flaw centroid.[9] To explore the applicability of a similar relationship to fatigue cracks, the magnetic perturbation signal peak separation was measured as a function of crack length on several specimens. These results are plotted in Figure 10 through 12. The data plotted in these figures were obtained for scan tracks over the centers of the cracks in Specimens S5, S29, and S30 for the high field condition. For clarity, the estimated measurement error bar is shown for only one data point in each figure. Also, only the data for zero load and the maximum applied static load are plotted for specimens S5 and S30, although data were also obtained for intermediate loads. No magnetic perturbation signals for the inclusions in Specimens S5, S29, and S30 were obtained prior to crack initiation. Therefore, to obtain a more informative trend line for the fatigue crack data, the average peak separation typically observed for inclusions from other investigations[9] is shown at zero crack length in Figures 10 through 13. The solid lines in Figures 10 through 13 were drawn to indicate data trends including the fatigue crack data and the inclusion data. It is apparent from these results that peak separation is dependent on crack length. Since the crack depth is directly proportional to the length for half-penny shaped cracks, the results reported here imply

7/9/76   SPECIMEN:S-5   MATERIAL:4340 STEEL
CRACK LENGTH:0.052"   NO. CYCLES: 9900
LOAD:FL FL=180KSI FIELD:HF   COMMENTS:CRACK "B"

4092

+ PRIN.

▲ SAT.

CRACK

HF

LF

P/P. SEPERATION (MILS)

SCAN TRACK LOCATION (DEG) (1 DEG ≃ 0.002 in.)

45   40   35   30   25   20   15   10   5   0   -5

250   260   270   280   290   300   310
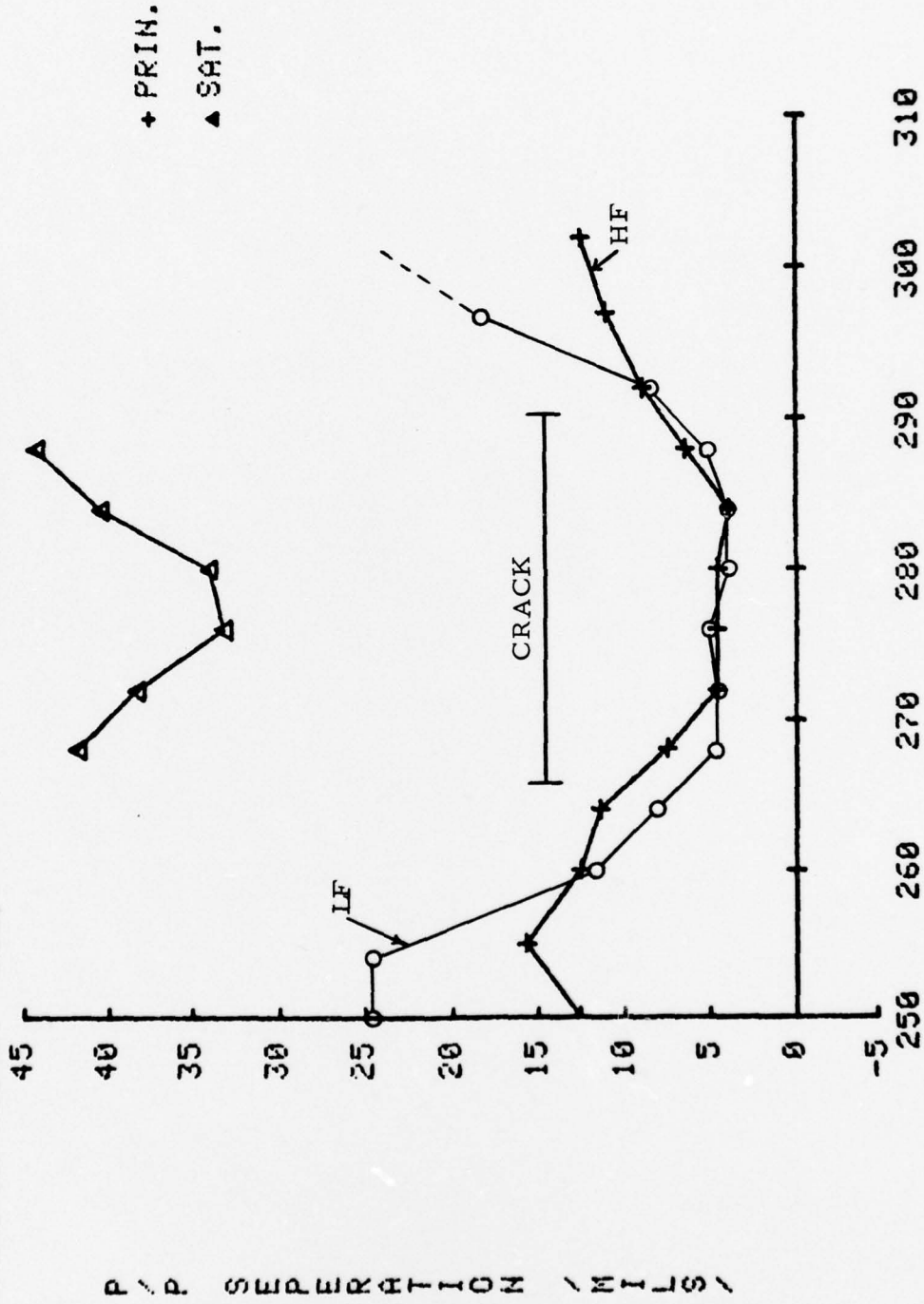
FIGURE 9.   MAGNETIC PERTURBATION SIGNAL PEAK SEPARATION
VERSUS LOCATION ALONG A CRACK INTERFACE.

FIGURE 10. PEAK SEPARATION OF MAGNETIC PERTURBATION PRINCIPAL COMPONENT AT CRACK CENTER VERSUS CRACK LENGTH. Specimen S5
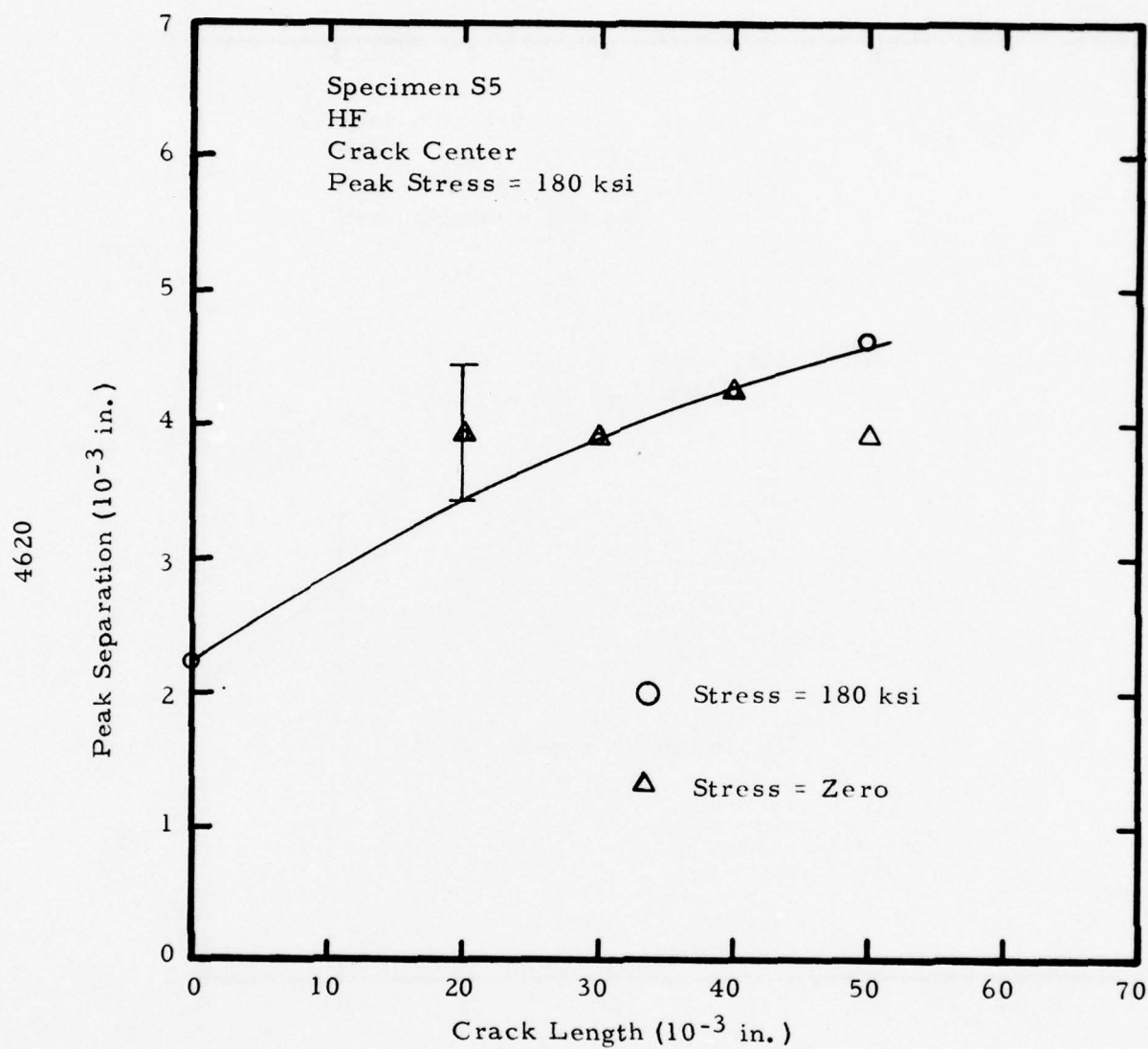
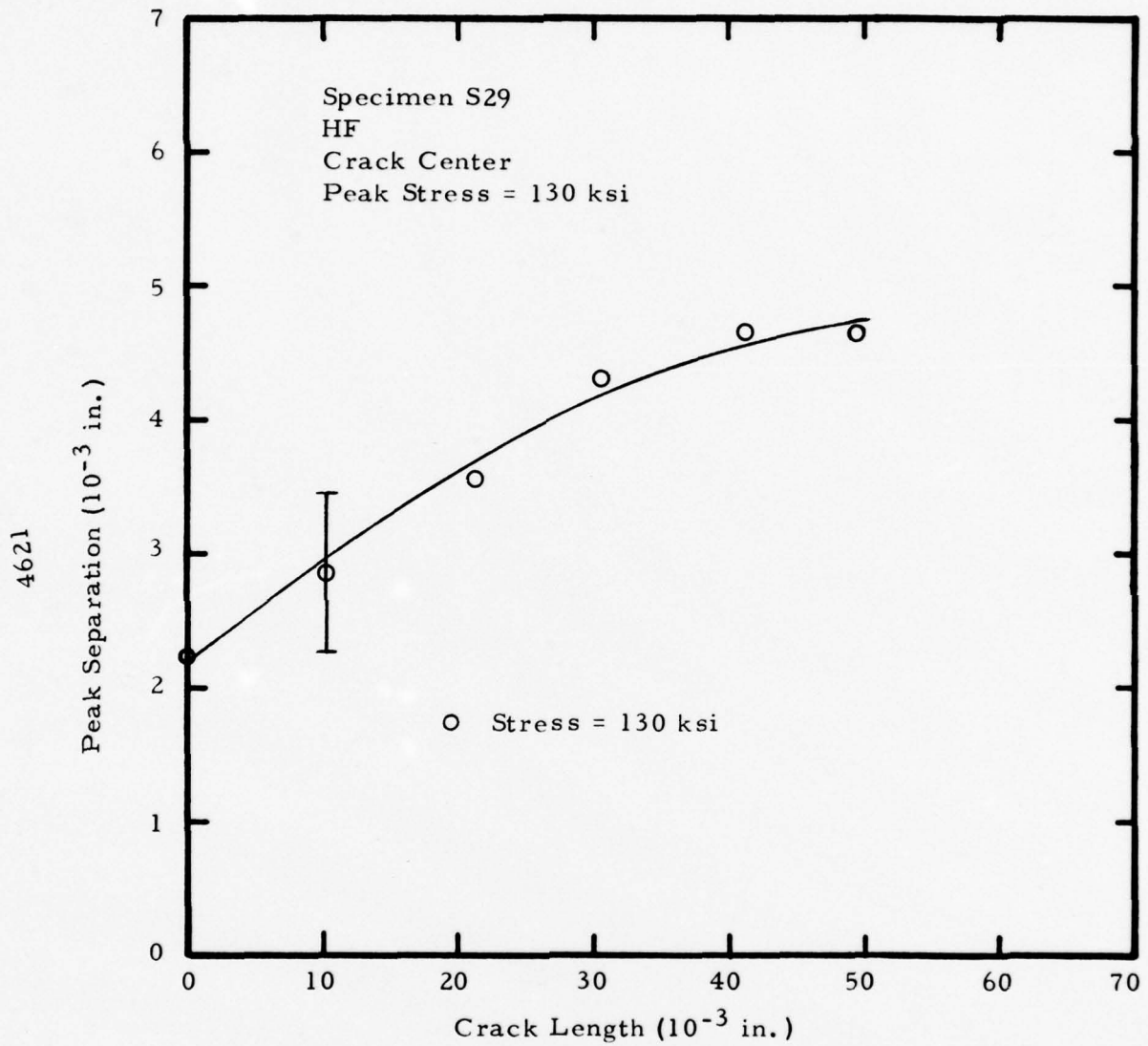FIGURE 11. PEAK SEPARATION OF MAGNETIC PERTURBATION
PRINCIPAL COMPONENT AT CRACK CENTER
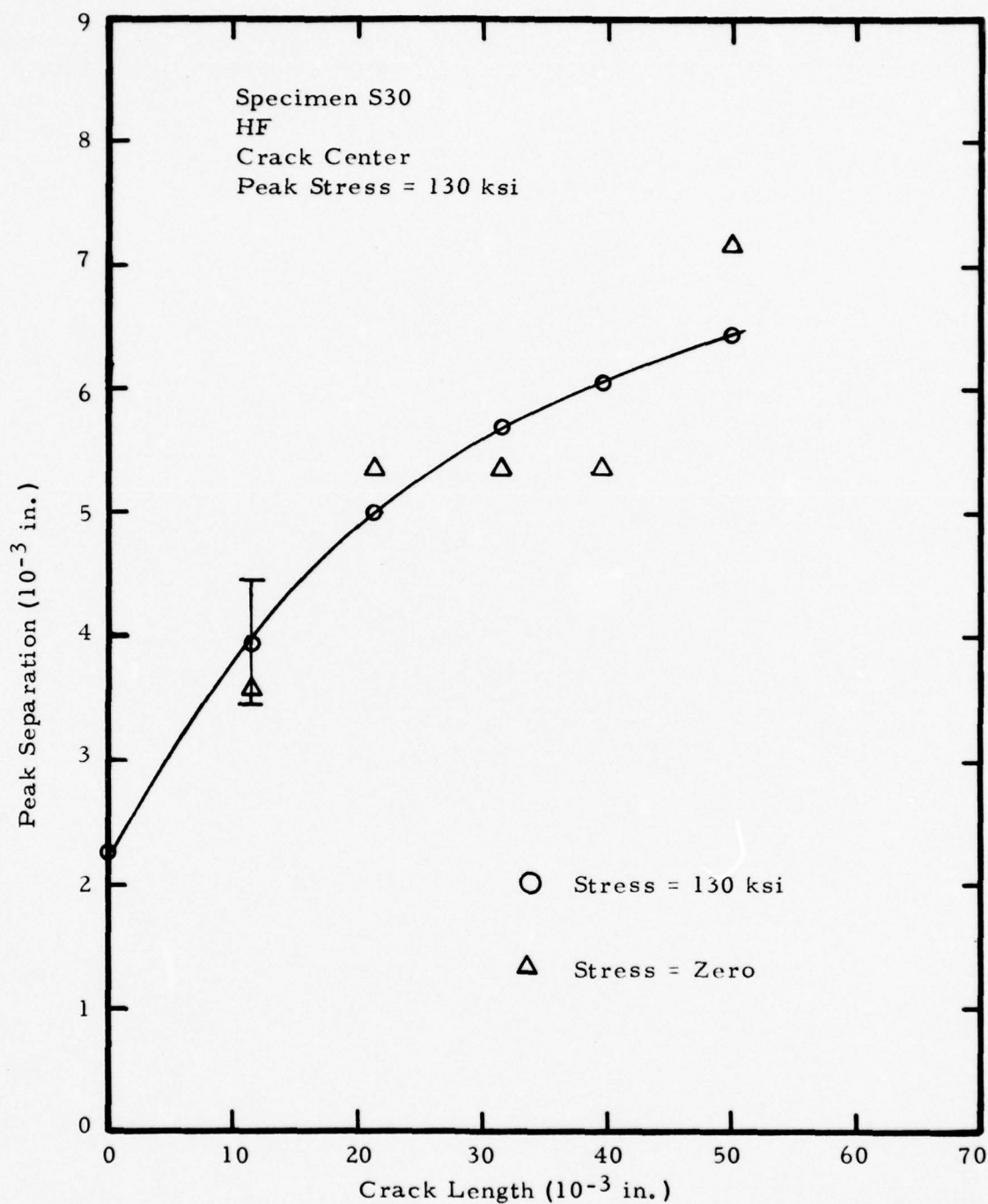VERSUS CRACK LENGTH. Specimen S29

FIGURE 12.   PEAK SEPARATION OF MAGNETIC PERTURBATION
PRINCIPAL COMPONENT AT CRACK CENTER VERSUS
CRACK LENGTH.   Specimen S30

that the magnetic perturbation signal peak separation is not simply linearly related to the crack depth as it is for inclusions but rather by a more complex relationship. Additional research is necessary to better define this relationship for fatigue cracks.

In further exploring the behavior of the magnetic perturbation signal peak separation, Figure 13 shows this parameter obtained along scan tracks approximately 6×10^{-3}-in. inside the crack tips plotted against crack length for Specimen S5 which was cycled at a stress level near yield. Note that for these scan tracks near the crack tips, the signal peak separation changes more with crack length than for scan tracks over the crack center (compare Figure 10), even though the change in crack depth with length is greater at the center than at the tip. Because of the high stress level at which the specimen investigated was cycled, the results observed for the magnetic perturbation signal peak separation at the crack tips may be associated with the severely worked plastic zones around the fatigue crack. This, however, has not yet been shown conclusively.

As is noted in the results presented in Figures 10 and 12, within limits of the experimental measurements, the magnetic perturbation signal peak separation does not change as the applied stress is changed from zero to its maximum value. This result is shown more clearly in the data presented in Figure 14 for Specimen S29. As is seen, the signal peak separation is essentially independent of applied load despite the fact that the magnetic perturbation signal amplitude increases by a factor greater than 9 over the same range (see Figure 6).

The development of analytical models should provide the basis for a more complete explanation of the behavior of magnetic perturbation signals in terms of magneto-mechanical interactions in the fatigue crack region. Initial attempts at such a model will be described in Section D.

B.   Comparison of Ultrasonic Responses from HY 180 and AISI 4340 Steel Specimens

Although only limited ultrasonic data were acquired, a comparison of the responses obtained from AISI 4340 with HY 180 shows significant differences. Figure 15 shows a comparison between ultrasonic pulse-echo reflections obtained from drilled holes 0.02-in.-diameter by 0.02-in.-deep in the two materials. Note that the signature from the hole in HY 180 is slightly lower in amplitude than for the identical size hole in AISI 4340; also, the background (material) noise in HY 180 is approximately a factor of 2 to 3 times higher in amplitude than the background noise in

FIGURE 13. PEAK SEPARATION OF MAGNETIC PERTURBATION
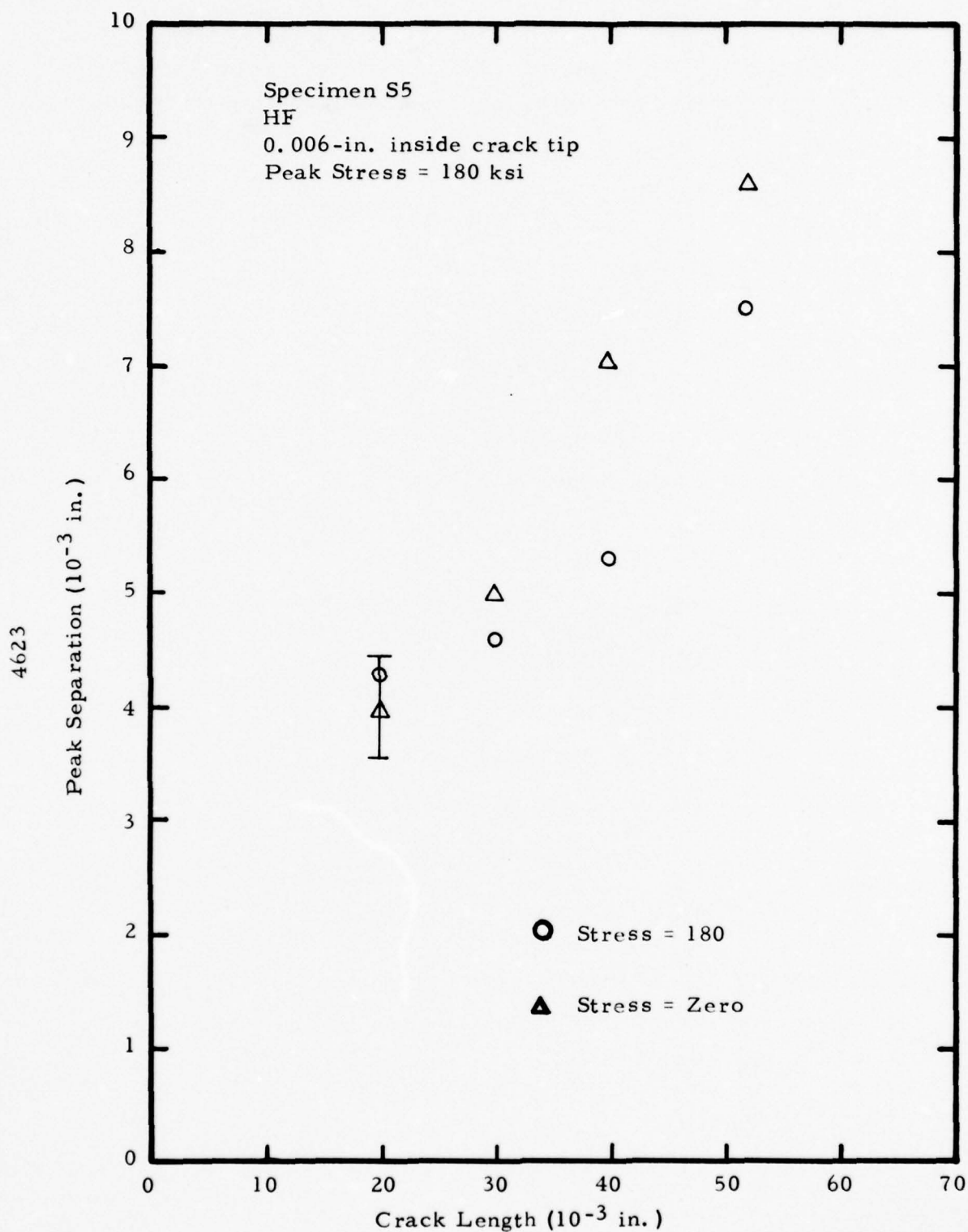PRINCIPAL COMPONENT 0.006-IN. INSIDE CRACK
TIP VERSUS CRACK LENGTH. Specimen S5

4624

Specimen S29; crack center
HF
Crack Length = 0.050-in.
σ_p = 130 ksi
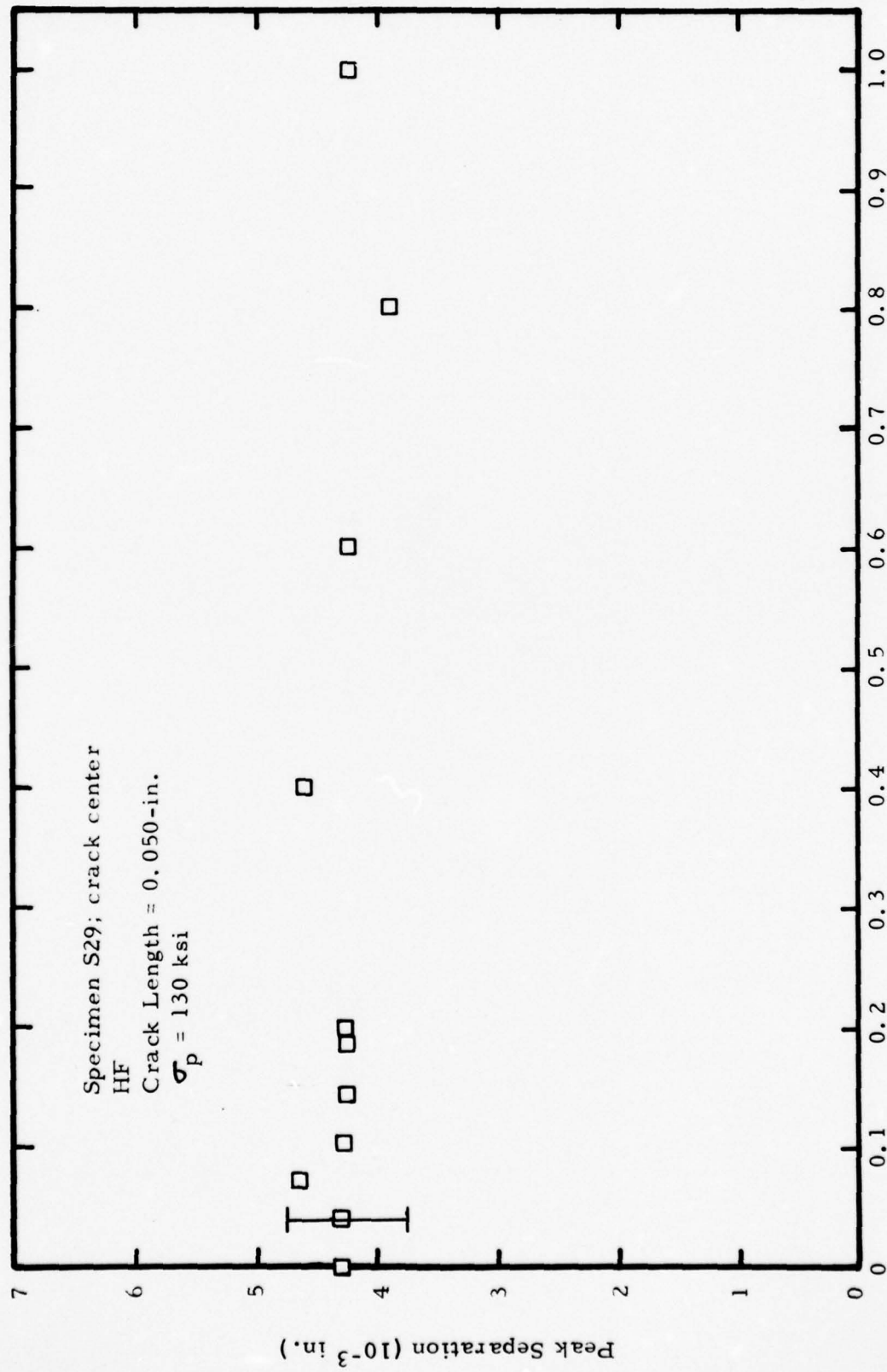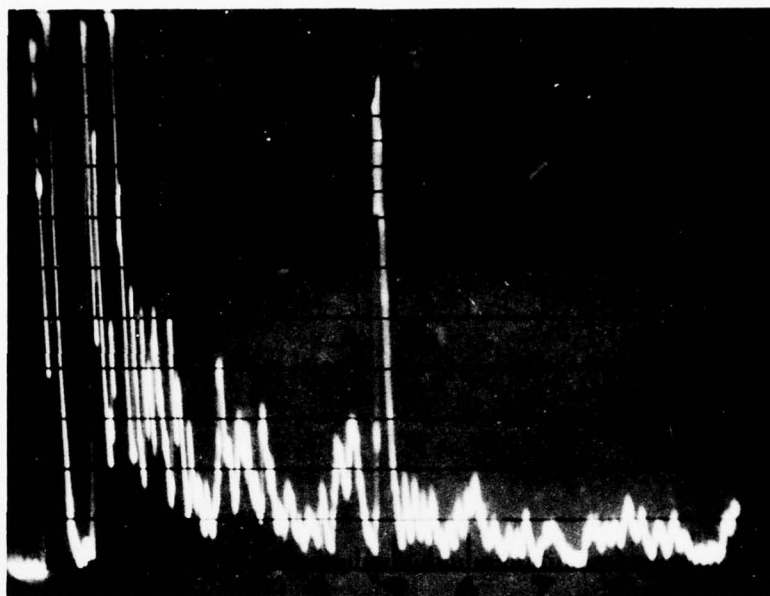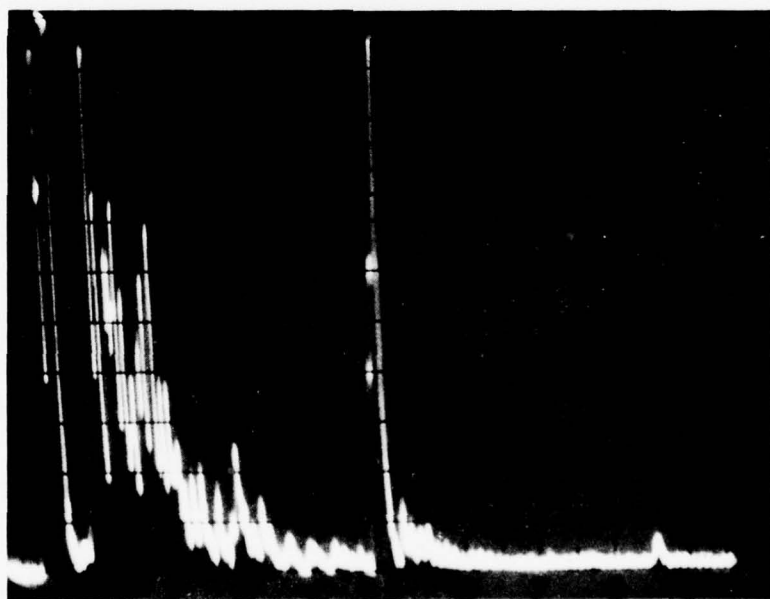
Peak Separation (10^{-3} in.)

FIGURE 14. MAGNETIC PERTURBATION PRINCIPAL COMPONENT PEAK
SEPARATION VERSUS APPLIED STRESS

a. HY-180

4380

b. AISI 4340

FIGURE 15. ULTRASONIC PULSE-ECHOES FROM A DRILLED HOLE

AISI 4340. Accordingly, it can be concluded that the smallest size geo-
metric discontinuity detectable in HY 180 using ultrasonic surface waves
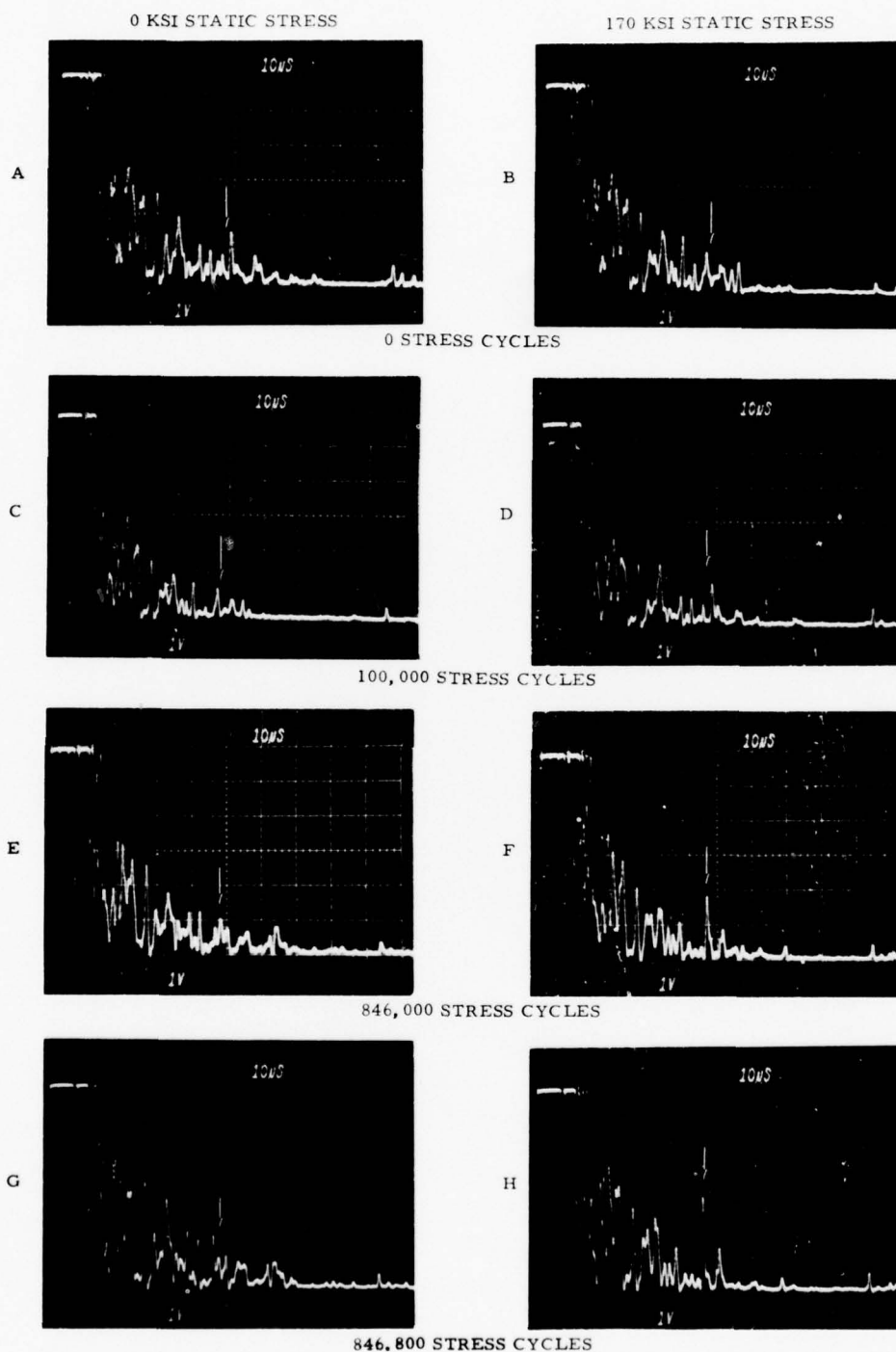at 10 MHz is approximately 3 times the minimum flaw size detectable in
AISI 4340.

Comparative ultrasonic results obtained from small fatigue
cracks are presented in Figures 16 and 17. For HY 180, analysis of the
ultrasonic records in Figure 16 indicates that a crack was first detected
at 846,000 stress cycles (Record F); at this time the crack length, deter-
mined by examination through the microscope, was approximately 0.026-in.
Even with a crack this long, it was necessary to apply load to obtain a
detectable ultrasonic response; the no-load indication was nil (see Record E).
The crack was propagated and after 800 more cycles the signature in
Record H, was obtained; at this time the crack was approximately 0.030-in.
long. By comparing Record G and H, it can be seen that for this crack length
also, no ultrasonic signature is discernible above the background (material)
noise under no-load conditions and that it is still necessary to apply load to
detect the crack. Also, the ultrasonic background varies somewhat during
cycling and could prevent detection of small cracks based on observations
of slight dynamic changes in specific background signatures. A similar
sequence of records obtained from an AISI 4340 steel specimen is shown
in Figure 17. Note the prominent signatures in Records F and H, and by
comparison the slight signature pointed out by the arrow in Record D. Also
note the almost perfect repeatability of the background signals. It is apparent
from Record G that even with no-load applied to the specimen, a prominent
signature is detected at 751,300 stress cycles when the crack is approximately
0.02-in. long. At 731,200 stress cycles, examination of Records C and D
indicates a slight change in signal with and without load applied when the
crack is only 0.0037-in. long, which is the limit of detection by ultrasonic
surface waves with stress applied.

These comparative results of ultrasonics experiments on
AISI 4340 and HY 180 indicate that while cracks 0.025-in. long can be
detected by conventional pulse-echo surface wave techniques in AISI 4340
without applying load, in HY 180, is is essential to apply load in order to
detect cracks even as long as 0.030-in.

C.   Metallurgical Investigations

1.   Microstructure

Investigations were conducted to determine whether
microstructural differences could account for the variations in ultrasonic
and magnetic perturbation responses observed between HY 180 and AISI 4340
steels. Sections were taken from the heat treated steels and were polished

0 KSI STATIC STRESS   170 KSI STATIC STRESS

A   B

0 STRESS CYCLES

C   D

100,000 STRESS CYCLES

E   F

846,000 STRESS CYCLES

G   H

846,800 STRESS CYCLES

NOTE: VERTICAL SENSITIVITY - 1 V/cm
       HORIZONTAL SWEEP - 10 μsec/cm

FIGURE 16.   ULTRASONIC SURFACE WAVE SIGNATURES FROM
FATIGUE CRACK IN HY 180 STEEL

O KSI STATIC STRESS   130 KSI STATIC STRESS

O STRESS CYCLES

731,200 STRESS CYCLES

742,850 STRESS CYCLES

751,300 STRESS CYCLES
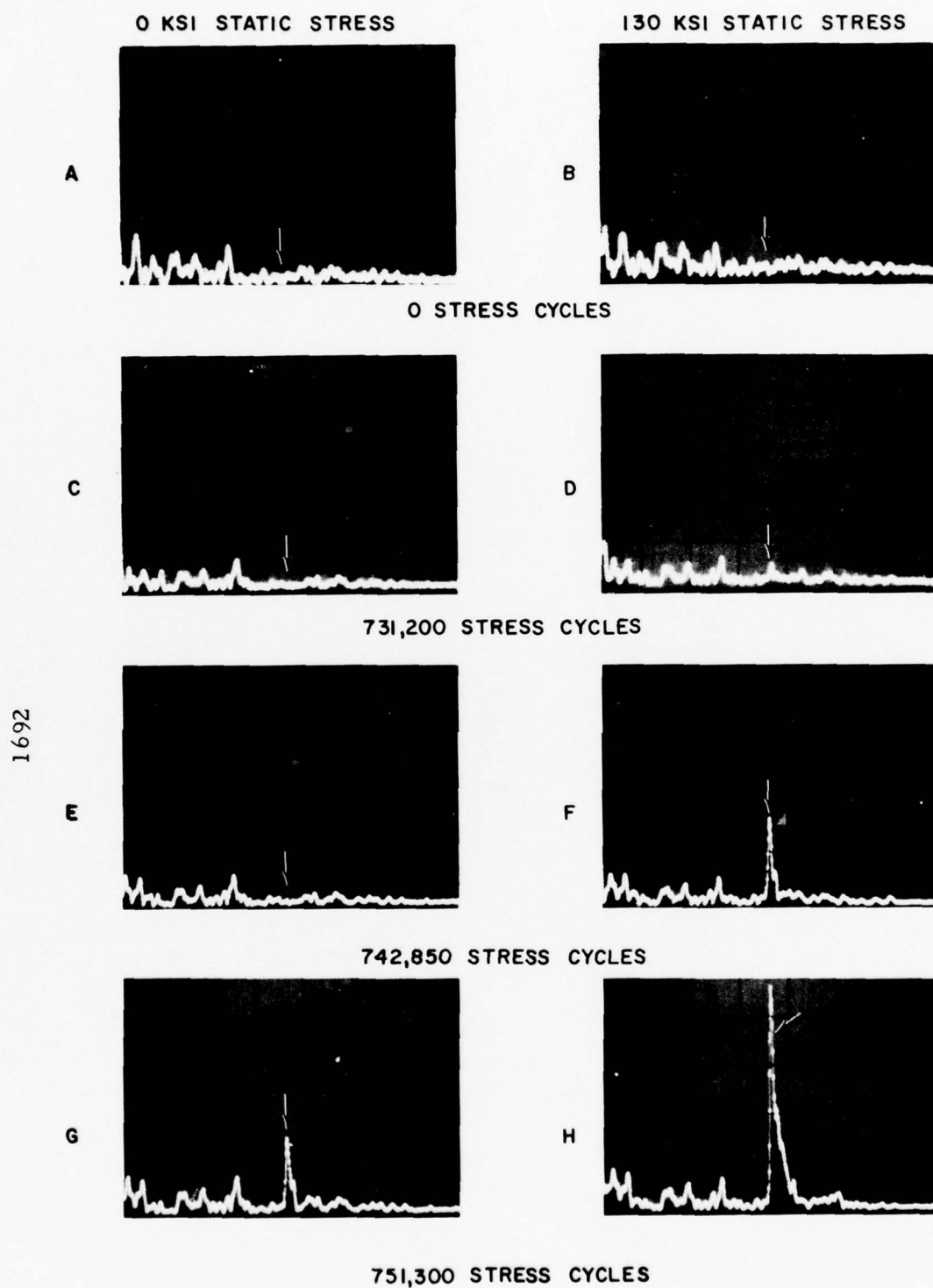
NOTE: VERTICAL SENSITIVITY-25 mv/cm
HORIZONTAL SWEEP-10 μsec/cm

FIGURE 17.   ULTRASONIC SURFACE WAVE SIGNATURES FROM
FATIGUE CRACK IN AISI 4340 STEEL

and etched in nital. The resulting microstructures are shown in Figure 18. As would be expected on the basis of the prescribed heat treatments (see Appendix C) the AISI 4340 microstructure consists of tempered martensite while the HY 180 steel is bainitic. In the latter case, the bainite colonies appear to delineate the prior austenite boundaries.

There are several differences between martensite and bainite which may account for the different NDE responses observed. While bainite like martensite is a dispersion of minute particles of carbide in ferrite as a continuous matrix, the ferrite of bainite is cubic in structure, not tetragonal as is martensite. Bainite, moreover, forms comparatively slowly by nucleation and growth at constant temperature, unlike martensite which forms almost instantly during a rapidly falling temperature. For this reason bainite tends to be free of microcracks. In many bainitic steels the cementite can precipitate within the ferrite laths as well as along the boundaries; cementite in tempered martensite is located totally at martensite plate boundaries. The habit planes for cementite formation often differ for bainite and martensite. Finally, the bainitic cementite structure seems to be more "blocky", like very fine pearlite, than the martensite microstructure of continuous carbide sheets adjacent to the laths.

Any or all of these microstructural considerations could possibly contribute to the observed differences in the acoustic and magnetic properties between AISI 4340 and HY 180 steels. For example, the "blocky" cementite structure in HY 180 and the tendency for the cementite to precipitate within the ferrite laths, could contribute to the higher acoustic background (material) noise observed in HY 180 compared to AISI 4340. In addition, the microstructure may be expected to influence the magneto-elastic characteristics, thereby causing the different magnetic perturbation responses observed between the two materials. Verification of these suggestions requires further investigation into the effects of various micro-structures on acoustic and magnetic properties.

2. Fractography

In this section, a brief comparison of fatigue crack initiation in the two materials AISI 4340 and HY 180 steel is presented. Figure 19 shows the macroscopic fractography of an AISI 4340 specimen (S5) and a HY 180 specimen, each cycled at a peak stress of 180 ksi. The specimens were cooled to -78°C by packing in dry ice and fractured using a standard tensile machine. In the case of the AISI 4340 specimen (Figure 19a), two fatigue cracks (arrows) coalesced during the final stages of fracture. It is apparent that the two grew stably, independent of one another, as half-penny shaped cracks. The nuclei of the cracks are shown in Figure 20 (arrows) and can be seen to be large (0.001-in.-diameter) spherical
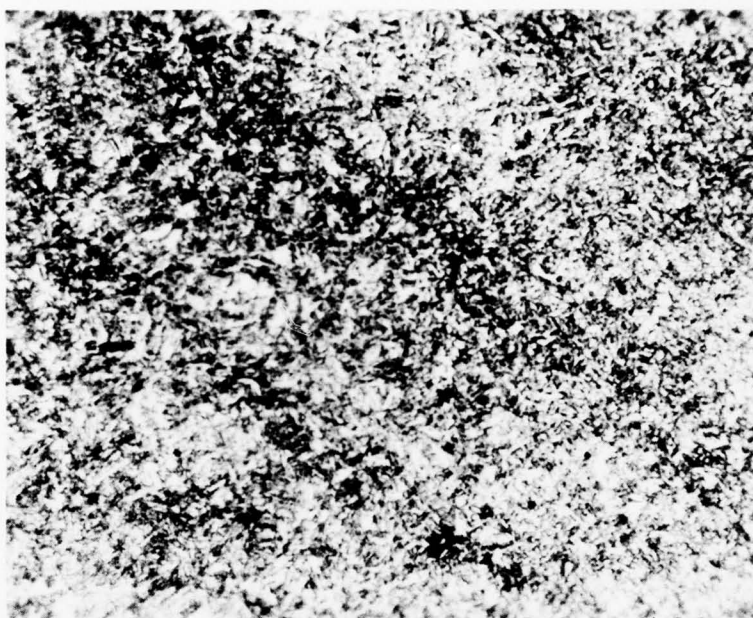
(a) AISI 4340 Steel - Martensitic. Magnification 500X

4625

(b) HY 180 Steel - Bainitic. Magnification 500X

FIGURE 18. METALLURGICAL MICROSTRUCTURES FOR AISI 4340
AND HY 180 STEEL

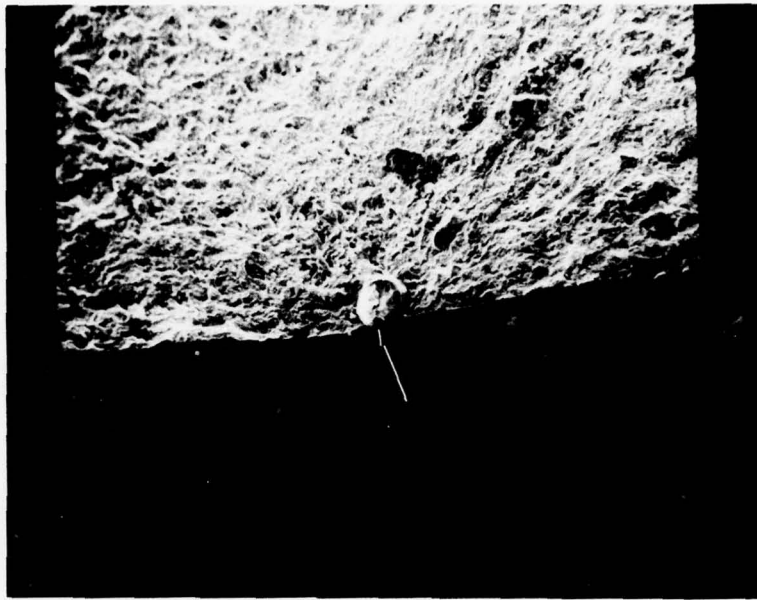(a) AISI 4340 Steel Specimen S5. Arrows Indicate
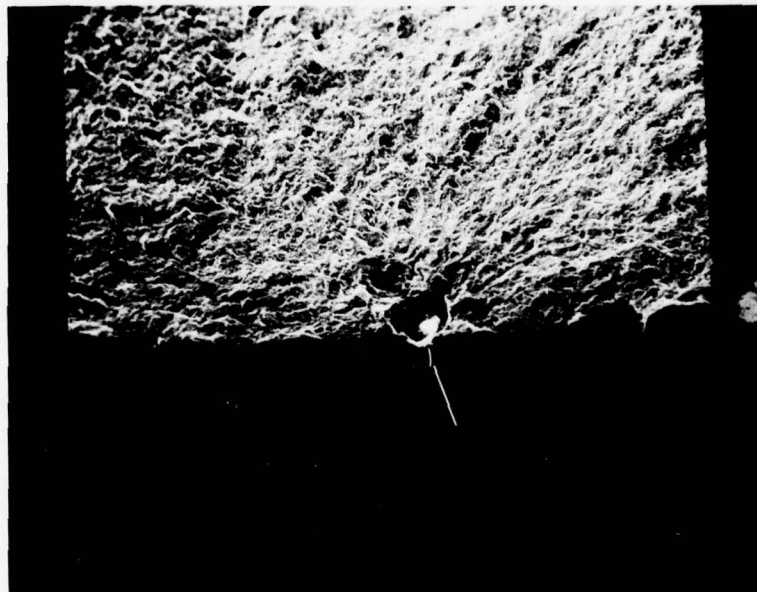Fatigue Cracks. Magnification 12.8X

4626

(b) HY 180 Steel Specimen H1. Magnification 12.8X

FIGURE 19. FRACTURE SURFACES FOR AISI 4340 AND HY 180 STEEL

4627

(a) Crack No. 1. Magnification 240X

(b) Crack No. 2. Magnification 240X

FIGURE 20.   FATIGUE CRACK INITIATION SITES IN AISI 4340
STEEL (Specimen S5).   Arrows indicate inclusions

nonmetallic inclusions. Although not investigated, their chemical makeup is probably duplex, that is, calcium aluminate and aluminum oxide.[2] Both inclusions, which touched the surface, appear to have fractured during stress cycling, although closer examination indicates that debonding also took place.

Only a single fatigue crack was involved in the HY 180 fracture, as is seen in Figure 19b. This crack also grew as a half-penny, but exhibited considerably more ductility at failure than was the case in the AISI 4340 material; note the evident necking which occurred about the crack. Also, unlike AISI 4340, the failure nucleus was not an inclusion but rather a small pore (0.0003-in. maximum dimension) which apparently was just barely open to the surface. The pore shown in Figure 21 was located at the origin of the river markings indicated by the arrow in Figure 21a. No significant differences could be discerned through fractography in the crack growth behavior of the two alloys.

3.   Plastic Zone Size

To obtain best characterization of fatigue cracks, it is important to know the distance over which it might be expected that the NDE inspection probes would be affected by the plastic zones at the fatigue crack tips. Accordingly, the approximate crack-tip plastic zone dimensions were determined in an AISI 4340 steel specimen using the microhardness approach. This technique recently has been applied with apparent success to both maraging steels and to austenitic stainless steels.[10] Because of the high strength of the former steels (which are similar to both AISI 4340 and HY 180 steels), the fatigue process induces cyclic softening within the plastic zone. Softening is, therefore, what might be expected in the AISI 4340 and HY 180 steel specimens. The specimen selected for this study was cycled at 130 ksi and contained a 0.050-in.-long crack such that the average stress intensity factor along the crack tip had been approximately 43 ksi$\sqrt{\text{in.}}$ The microhardness profiles, obtained at depths of 0.001-in. to 0.002-in., 0.002-in. to 0.003-in., and approximately 0.010-in., are summarized in Figures 22, 23, and 24.

Near the surface (Figure 22) the hardness readings indicate fatigue hardening in both directions relative to the crack plane. Parallel to the crack plane the apparent plastic zone boundary lies at about 0.010-in. while perpendicular to the crack plane the boundary is about 0.012-in. away. Slightly deeper within the specimen a shift in this trend is observed. As shown in Figure 23 hardness readings normal to the crack plane from two directions show in one case no change at all (Figure 23a) and in another case a slight softening (Figure 23b); in the latter instance, the boundary lies at about 0.010-in. Readings obtained parallel to the plane of the crack for this
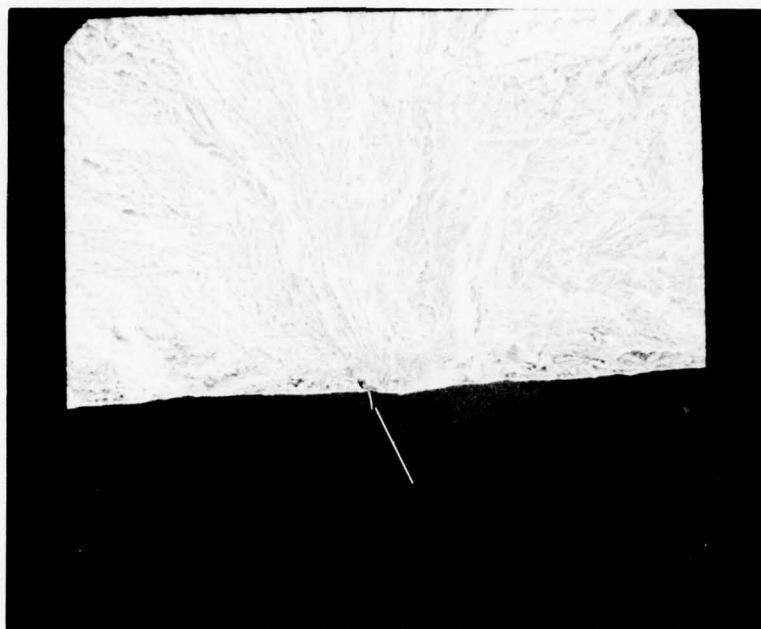
(a) Magnification 285X

(b) Magnification 2850X

FIGURE 21.   FATIGUE CRACK INITIATION SITE IN HY 180 STEEL
Specimen H1
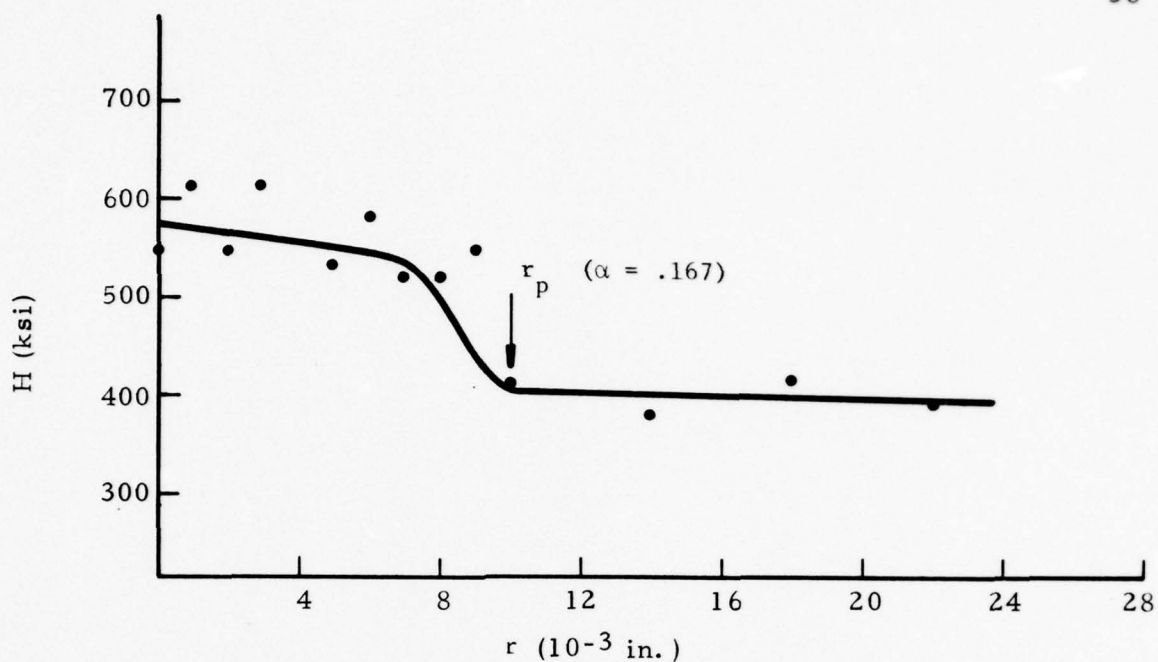
(a) Microhardness Profile Parallel to Crack Plane

4629
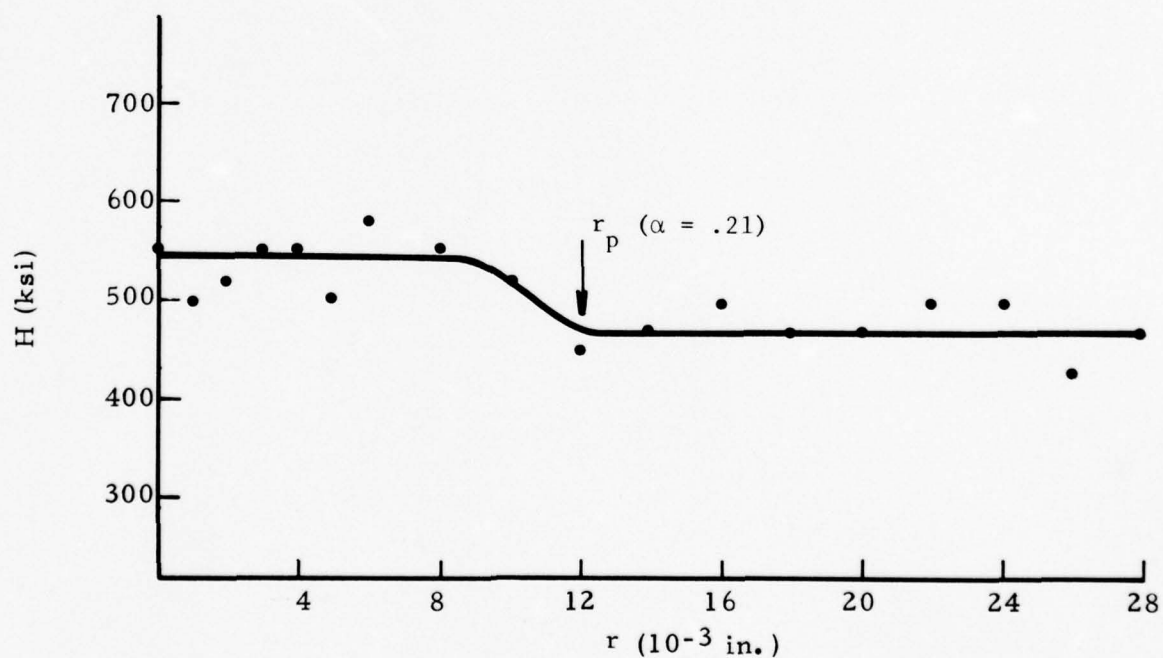
(b) Microhardness Profile Perpendicular to Crack Plane

FIGURE 22. NEAR SURFACE (0.001-0.002-in.-deep) PLASTIC ZONES
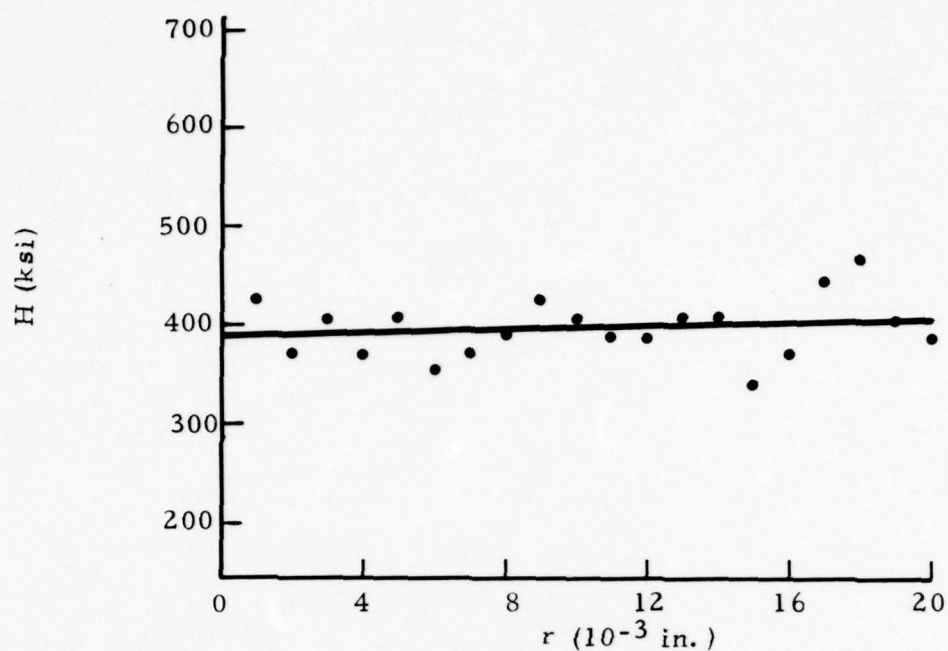
(a) Microhardness Profile Perpendicular to Crack Plane
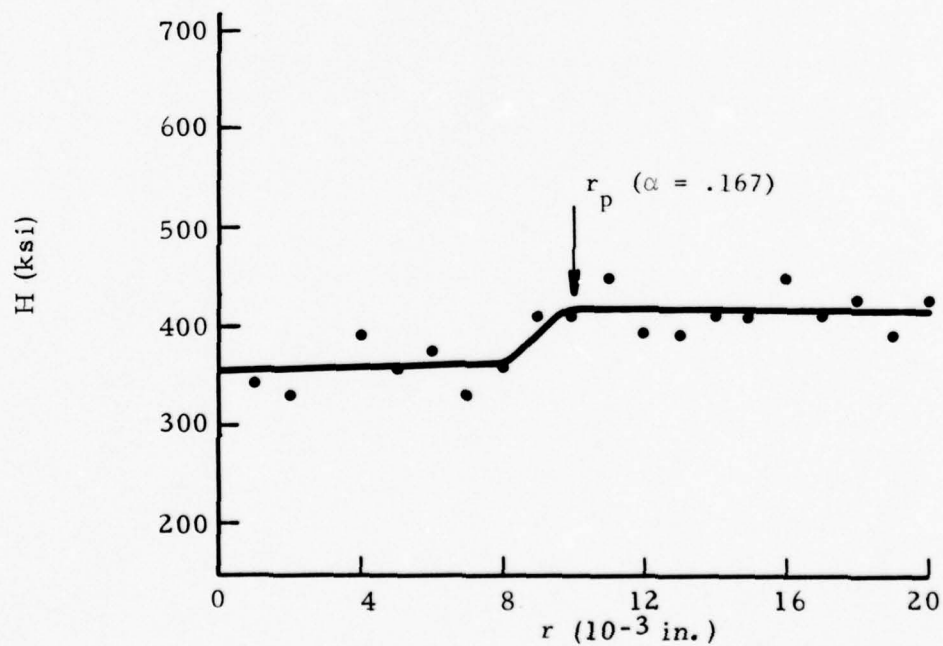
(b) Microhardness Profile Perpendicular to Crack Plane

FIGURE 23. PLASTIC ZONES AT 0.002-0.003-IN. DEPTH
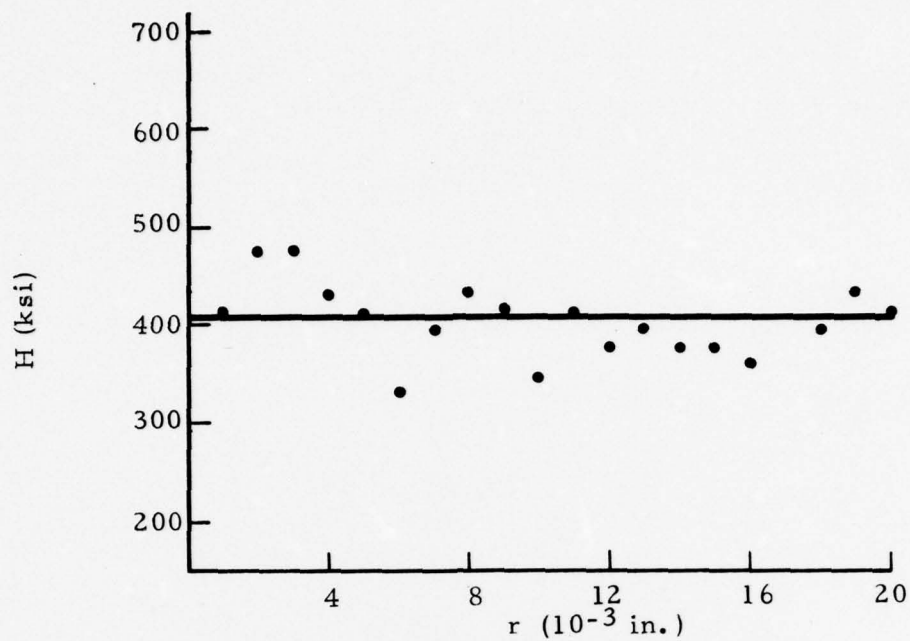
(a) Microhardness Profiles Parallel to Crack Plane
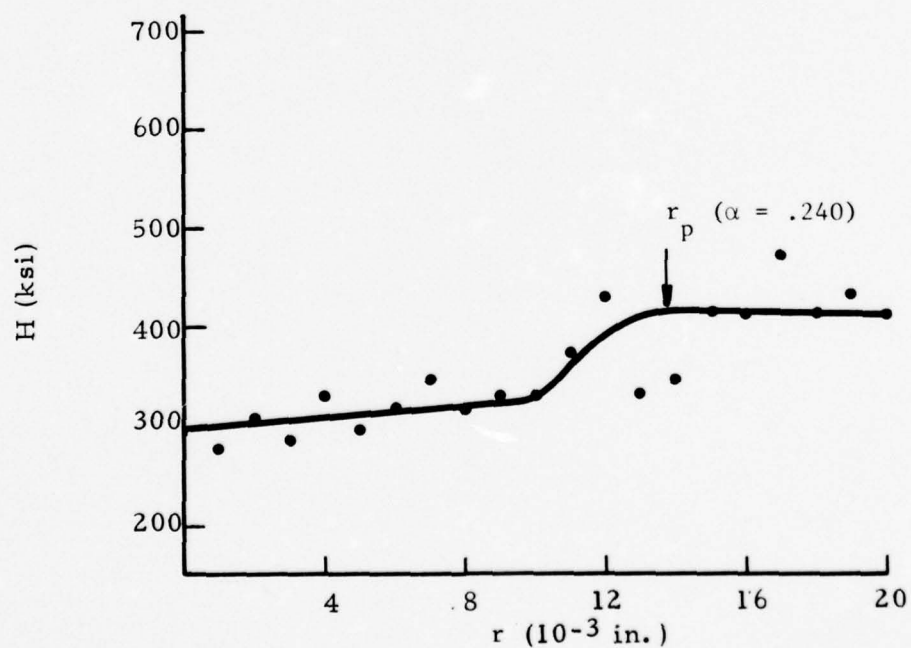
(b) Microhardness Profiles Perpendicular to Crack Plane

FIGURE 24. INTERIOR (0.010-in.-deep) PLASTIC ZONES

4631

depth indicated essentially no change in hardness. Finally, data obtained at a depth of 0.010-in. (Figure 24) show that softening again occurred normal to the crack plane but that no detectable plastic deformation has taken place immediately ahead of the crack.

Based on these observations, the following picture of the plastic zones in this specimen emerges. Near the surface, the plastic zone extends about equally both in front and to the side of the crack. This is in agreement with the generally accepted notion of a plane stress crack tip zone, as would be expected near the surface.[11] Deeper in the specimen the crack tip state of stress shifts to plane strain and the plastic zone shape is altered such that most of the strain field is accommodated above and below the plane of the crack with little strain in front of the crack.

The plastic zone size r_p can be described by[11]

$$r_p = \alpha \left(\frac{\Delta K}{\sigma_y} \right)^2 \tag{1}$$

where α is a constant, ΔK the stress intensity range, and σ_y the yield stress. According to theory[11], under plane stress conditions α should have a value ranging from 0.16 to 0.2 which is in good agreement with the values of 0.17 and 0.21 obtained for the near surface measurements. Under plane strain, the corresponding theoretical range in α for the direction perpendicular to the crack plane is 0.138 to 0.15 which can be compared with the experimental value obtained here of $\alpha = 0.24$. In the direction parallel to the crack, plane strain theory predicts $\alpha = 0.035$ to 0.1, whereas the experimental results is $\alpha \approx 0$.

The surface hardening and interior softening observed is surprising and has not been previously reported. No explanation for this phenomena can be given at this time pending further investigation on additional specimens. It is not obvious how merely changing the state of stress would affect so profound a change.

D. Analytical Characterization of Magnetic Leakage Fields Associated with Fatigue Cracks

The relationship between the magnetic perturbation signal characteristics and the parameters characterizing fatigue cracks implied by the results presented in the previous section suggest that a mathematical description of the magnetic leakage field associated with a realistic surface fatigue crack in a ferromagnetic steel would be extremely useful. Such a model would provide a capability for utilizing the detected magnetic signatures to infer directly the crack geometry and the loading parameters.

Unfortunately, complete treatment of the problem for a real fatigue crack, taking into account all factors of recognized significance, has not yet been accomplished. There are three basic conditions that would appear to be essential to an acceptable model: (1) the model must take into account, in at least an approximate manner, the known boundary conditions applying to the magnetostatic field (as prescribed by Maxwell's equations) and the elastic field (from the Navier equations); (2) the model must treat a crack of finite length, depth and crack opening displacement; (3) the model must take into account the fact that the magnetic permeability of the material is appreciably altered by plastic deformation in the vicinity of the crack front.

In the absence of a more realistic mathematical model along the lines of that described above, a preliminary analysis has been published[12] in terms of a simple model which treats a crack as an infinitely long surface slit of rectangular cross-section and supposes the magnetic leakage field to arise solely from a uniform distribution of magnetic charge over the parallel faces of the crack, the charge being of opposite sign on opposing faces. Since this model meets only the first of the aforementioned three conditions of a fully acceptable model, the results obtained using it must be interpreted with due caution.

In an attempt to take into account crack geometry, the simple model described in Ref. 12) has been modified in an approximate way to apply to a surface flaw whose geometry is shown in Figure 25. The crack is assumed to be a half-penny shape with length 2c and depth at the center c. It is open under the action of a remote static stress σ_∞. The maximum crack opening displacement is at x=0, y=0 and for a linearly elastic body is given approximately by[13]

$$2\Delta = COD = 2kc\sigma_\infty \tag{2}$$

where

$$k = \frac{(1-\nu^2)(\pi+2)}{\pi E} \tag{3}$$

ν is Poisson's ratio and E is Young's modulus. The shape of the flaw on the surface may be described approximately by two parabolic curves intersecting at the crack tips (y=±c) and separated by a distance 2Δ, the crack opening displacement at y=0. If the crack opening at any distance y along the crack is designated by 2δ then

$$\delta = \Delta\left[1 - \left(\frac{y}{c}\right)^2\right] \tag{4}$$
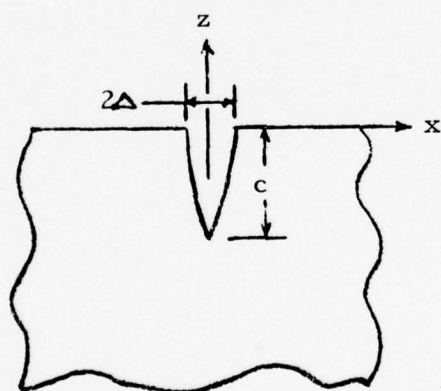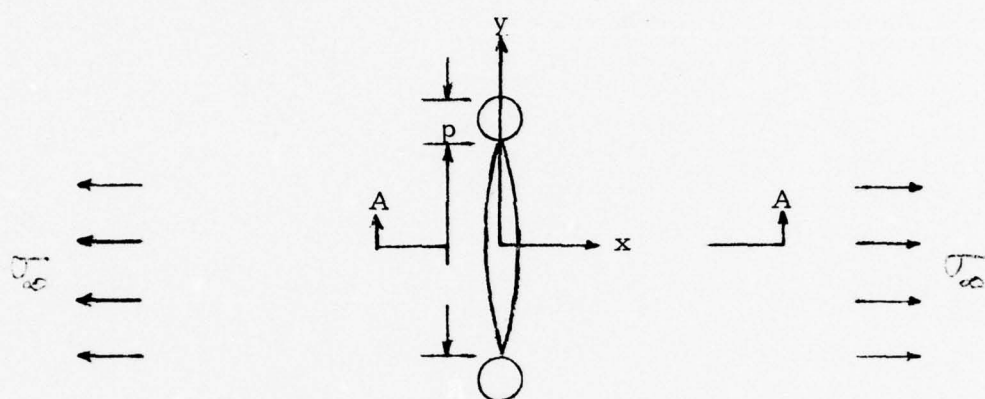
FIGURE 25. SURFACE FLAW GEOMETRY

Combining equations 2 and 4 results in

$$\delta = k c \,\sigma_{\!\infty} \left[1 - \left(\frac{y}{c}\right)^{2} \right]$$

<div align="right">(5)</div>

The depth of the crack, d, varies along the crack length as

$$d = c \cos\left(\frac{\pi y}{2c}\right)$$

<div align="right">(6)</div>

Utilizing this approach the model described in Ref. 12 can be extended to allow computation of H_z, the component of magnetic leakage flux normal to the specimen surface for a surface flaw. Typical curves of the leakage flux as a function of distance along the crack interface as predicted by this model are shaped as the one shown in Figure 26 and agree in a qualitative sense with experimentally determined curves. In attempting to correlate predictions of the model quantitatively with experimental results, a discrepancy is found in the fact that the model predicts a vanishing leakage field at the crack tips, whereas experimentally the magnetic perturbation signal is found to extend out to distances of up to half a crack length beyond the crack tips (see Figure 5).

There are several possible reasons for this discrepancy. For example, the leakage flux may be expected to fringe at the crack tips, an effect not accounted for in the two dimensional "strip theory" approach which assumes the leakage flux vector field lies entirely in the x-z planes. It is almost certain that near the crack tips the magnetic flux is three-dimensional in character and that a signal amplitude should exist beyond the crack tips as observed experimentally. Another possible explanation is that at the crack tips, intense zones of (plane stress) plastic deformation are created, characterized on the microscale by void nucleation and coalescence and microcrack formation. These regions of intense slip and dislocation may in themselves promote flux leakage much as small surface cracks do. Also, an actual crack under load has a finite crack tip radius whereas the model assumes a zero radius. Finally, on a dimensional scale of the order of the plastic zone, the magnetic permeability may be expected to be changed significantly due to intense plastic straining from the values characteristic of the bulk material. This effect is also not accounted for in the present model.

In an attempt to bring the analytical model into better conformance with experimental results, it was modified by including a "process zone" so that a half-penny shaped crack of length 2 (c+p) is considered where p is the linear dimension of the process zone (see Figure 25). For purposes of computation, the quantity p is taken to be the plastic zone size estimated
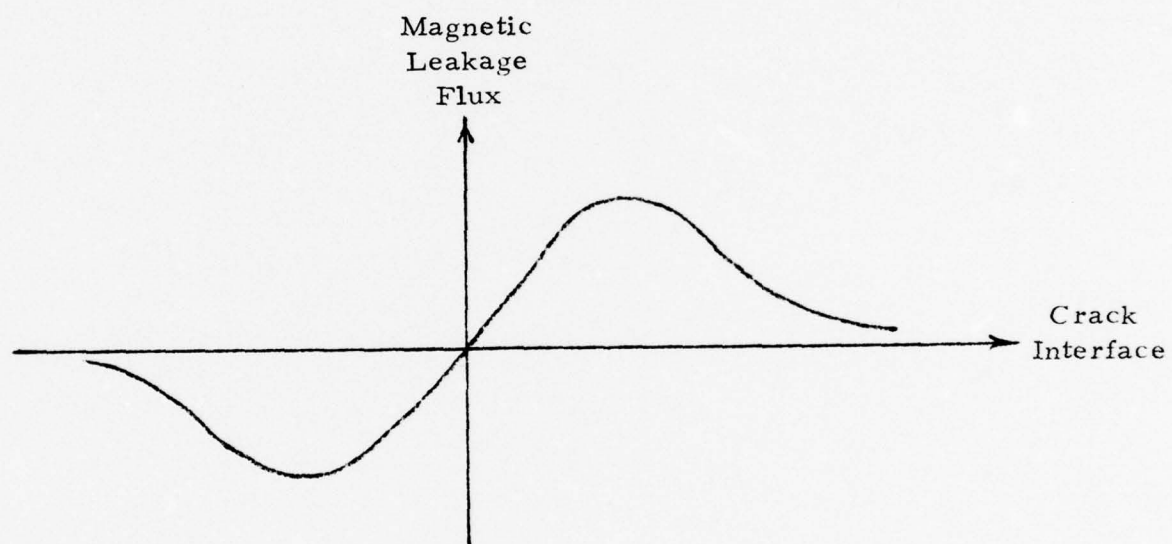
FIGURE 26. CALCULATED MAGNETIC LEAKAGE FLUX VERSUS
DISTANCE ALONG CRACK INTERFACE

from plane stress theory[14] as

$$\rho = 1.55 \, c \left(\frac{\sigma_{\infty}}{\sigma_Y} \right)^2$$

(7)

where σ_Y is the yield strength in simple tension. Utilizing this approach, predictions of the model for magnetic leakage flux were compared with experimental data obtained from specimens of AISI 4340 steel and HY 180 steel having small surface cracks. Low field data from three cracks approximately 0.03-in., 0.04-in., and 0.05-in. long were examined, each under five different applied stress levels for both specimens.

Some of the results obtained with the model are shown in Figure 27 compared with experimental data. These results are for a 0.03-in.-long crack in AISI 4340 steel Specimen S5. Plotted in Figure 27 is the magnetic perturbation signal amplitude versus location along the crack interface for several different static stress levels. In each case the computed curve was fitted to the experimental data at y=0. As can be seen, the agreement between the model predictions and the experimental data is reasonably good and the inclusion of a process zone correction into the model helps to account for the signal amplitude observed beyond the crack tip. Although the results shown here are for a 0.03-in. crack in an AISI 4340 steel specimen, similar results were found for other cases considered, including those in HY 180 steel.

The analytical model described here comprises a first step in developing a mathematical description of the magnetic leakage field associated with a realistic surface fatigue crack. The approach taken was to incorporate geometrical parameters characteristic of a half-penny shaped crack into a model for treating a crack of infinite extent. Although certain limited agreement with experimental results was obtained, to be useful in application to actual fatigue cracks, the model needs to take into account directly the magnetic, elastic, and plastic properties of the material in addition to the geometrical considerations of the fatigue crack. Thus, for a more complete mathematical description, analytical efforts should be directed toward magnetic flux leakage model for a surface crack of finite width and depth and having a crack opening field consistent with that given by elasticity and plasticity theory. In addition, the influence of plastic deformation in the vicinity of the fatigue crack on the magnetic permeability of the material must be taken into account. It is hoped that future work directed along these lines will result in the achievement of a more rigorous analytical model for the magnetic leakage flux in terms of the magneto-mechanical interactions in the fatigue crack region.

4634

Distance, y, from Crack Center (10^{-3} in.)
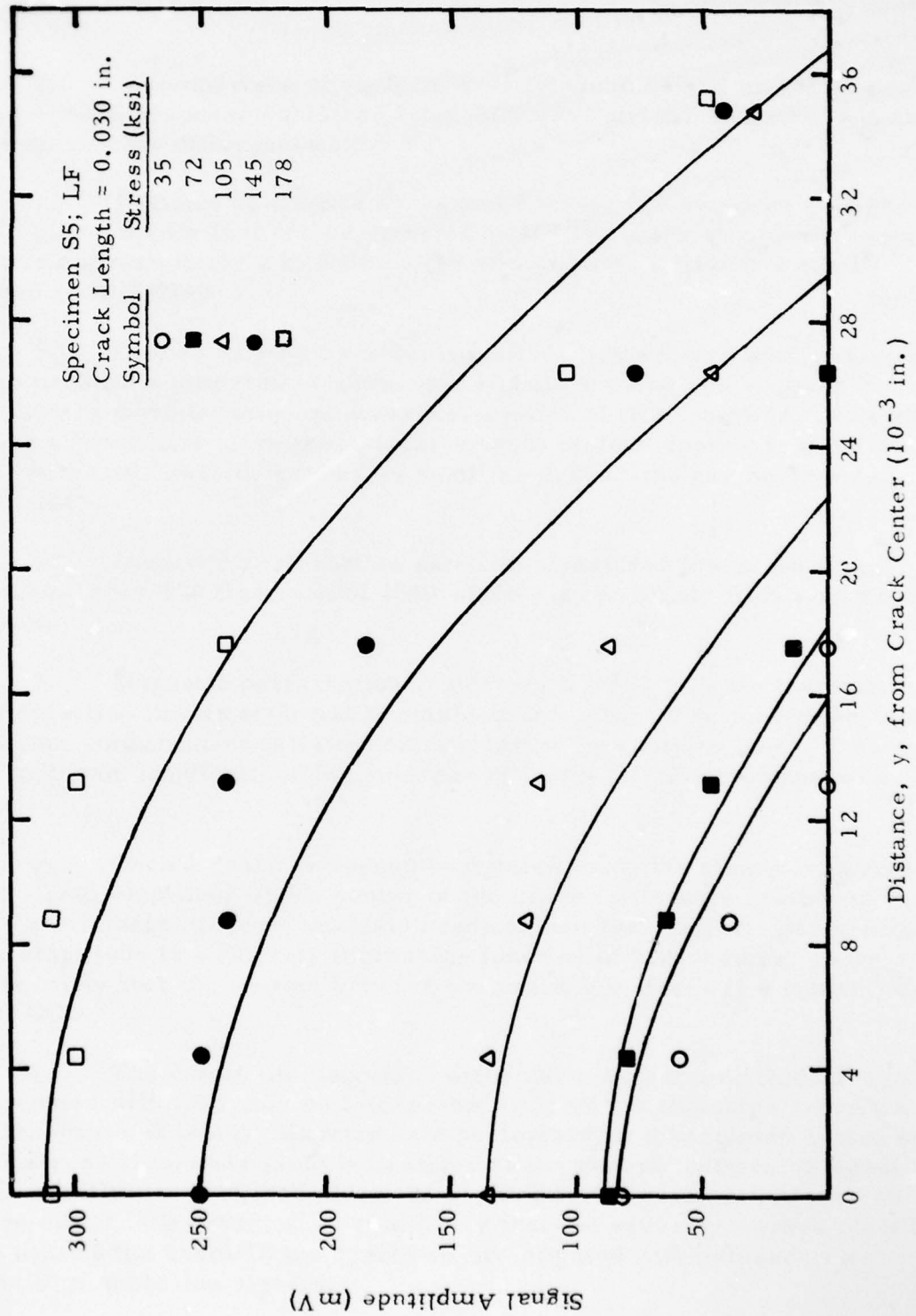
Signal Amplitude (mV)

FIGURE 27. EXPERIMENTAL AND CALCULATED MAGNETIC PERTURBATION SIGNAL AMPLITUDE VERSUS LOCATION ALONG CRACK INTERFACE FOR VARIOUS STRESS LEVELS

IV.   CONCLUSIONS AND RECOMMENDATIONS

The following conclusions can be made based on the results discussed in this report:

1.   A comparison of surface wave ultrasonics and magnetic perturbation NDE responses obtained from AISI 4340 and HY 180 steel specimens shows significant differences.

2.   Because of greater background noise, the smallest size geometric discontinuity that can be detected in HY 180 using ultrasonic surface waves is approximately 2 to 3 times the minimum size flaw that can be detected in AISI 4340.

3.   Cracks as long as 0.026-in. in HY 180 require application of load to produce a discernible ultrasonic signature using conventional pulse echo surface wave techniques, whereas, cracks of this length in AISI 4340 produce a prominent ultrasonic signature with no load applied to the specimen. With load applied, cracks as small as 0.0037-in. can be detected in AISI 4340.

4.   Magnetic perturbation satellite signatures are much more prominent in HY 180 than in AISI 4340 which may be an aid to fatigue crack detection.

5.   Magnetic perturbation results on HY 180 indicate that earliest crack detection in this material is obtained under high flux conditions, and significant enhancement of detection is obtained by applying load. This may have important implications for guidance of future Air Force inspection methods.

6.   Once a crack is opened by applied load, the magnetic perturbation signal amplitude at the center of the crack is linearly related to the COD. Since magnetic field analysis predicts that the magnetic perturbation signal amplitude is a linearly increasing function of void volume, these results imply that the volume between the crack interfaces is a linear function of COD.

7.   The change in magnetic perturbation signal amplitude at the crack center with load may be interpreted in terms of inclusion contributions and crack closure. Experiments performed on a specimen cycled at a peak stress level near yield indicated that the general pattern of signal change at different positions along the crack interface may imply a small closure effect. However, it is also likely that the severely worked plastic zones around the crack in the specimen investigated will influence the magnetic perturbation signals.

8.   Results obtained on several specimens indicate that for fatigue cracks, the magnetic perturbation signal peak separation varies with crack length in a nonlinear fashion. The behavior of the peak separation for fatigue cracks may be associated with plastic zones. This hypothesis is corroborated by the result that the peak separation is less for scans near the crack center than those near the tips where the stress zones are larger, and the peak separation near the crack tip varies considerably with crack length.

Recommendations for further research follow:

1.   Further explore the possible relationship between the magnetic perturbation signal peak separation and plastic zones around fatigue cracks.

2.   Perform comprehensive NDE investigation of specimens fabricated from AF 1410 steel (which is a higher fracture toughness version of HY 180) to determine parameters suitable for effective defect characterization. Compare responses of AF 1410 with AISI 4340 and HY 180 steel to provide guidance for future NDE inspection of AF 1410 components based on modifying procedures currently used for AISI 4340.

3.   Continue development of a refined and comprehensive mathematical model relating the flux leakage field produced by a true fatigue crack to parameters needed for determination of crack criticality by fracture mechanics analysis. Such a model should take into account the magnetic, elastic, and plastic properties of the material.

4.   Perform investigations on Ti-6Al-4V and superalloys to determine the parameters for effective defect characterization using stress enhanced surface wave ultrasonics, electric current injection, and AC four-contact electric probe methods.

5.   Develop the NDE methods cited in No. 4 above for application to specific inspection problems, such as, cracks around fastener holes, cracks in fan blades, and cracks in turbine disks.

6.   Conduct experimental and analytical effort to explore the potential of portraying defects using video displays reconstructed from characteristic features of magnetic perturbation signatures, and possibly electric current injection and AC four-contact electric probe signatures.

V.   PUBLICATIONS

The following papers have resulted from work conducted under AFOSR Contract No. F44620-75-C-0042:

(1)   "Critical Inspection of Bearings for Life Extention," J. R. Barton, F. N. Kusenberger, P. L. Hampton, and H. Bull, Proc. 10th Symposium on NDE, San Antonio, Texas, April, 1975.

(2)   "Magnetic Field Leakage due to a Surface Crack," W. L. Ko and P. H. Francis, Brit. J. Nondest. Test. <u>17</u>, 141 (1975).

(3)   "Advanced Quantitative Magnetic Nondestructive Evaluation Methods - Theory and Experiment," J. R. Barton, F. N. Kusenberger, R. E. Beissner, and G. A. Matzkanin, Twenty-Third Sagamore Army Materials Conference, Raquette Lake, New York, August 24-27, 1976.   Proceedings are in the process of being published.

The following reports have been published under AFOSR Contract No. F44620-75-C-0042:

(1)   "Nondestructive Evaluation of Metal Fatigue," F. N. Kusenberger, J. Lankford, Jr., P. H. Francis, and J. R. Barton, AFOSR-TR-76-0384, March, 1976.

(2)   "Nondestructive Evaluation of Metal Fatigue," F. N. Kusenberger, G. A. Matzkanin, J.R. Barton, and P. H. Francis, AFOSR-TR-77-0191, February, 1977.

VI.   REFERENCES

1.   Kusenberger, F.N., Lankford, J., Francis, P.H., and Barton, J.R., "Nondestructive Evaluation of Metal Fatigue," Final Scientific Report AFOSR 70-1206TR, March, 1970.

2.   Kusenberger, F.N., Matzkanin, G.A., Barton, J.R., and Francis, P.H., "Nondestructive Evaluation of Metal Fatigue," Final Scientific Report AFOSR-TR-75-0937, March, 1975.

3.   Kusenberger, F.N., Francis, P.H., Leonard, B.E., and Barton, J.R., "Nondestructive Evaluation of Metal Fatigue," Interim Scientific Report, AFOSR-69-1429TR, April, 1969.

4.   Kusenberger, F.N., Matzkanin, G.A., Barton, J.R., and Francis, P.H., "Nondestructive Evaluation of Metal Fatigue," Interim Scientific Report, AFOSR-TR-76-0384, March, 1976.

5.   Barton, J.R., Kusenberger, F.N., Beissner, R.E., and Matzkanin, G.A., "Advanced Quantitative Magnetic Nondestructive Evaluation Methods - Theory and Experiment," Twenty-Third Sagamore Army Materials Research Conference, August 24-27, 1976. Proceedings in print.

6.   Elber, W., "Fatigue Crack Closure Under Cyclic Tension," Engineering Fracture Mechanics, 2, 37 (1970).

7.   Ho, C.L., Buck, O., and Marcus, H.L., "Application of Strip Model to Crack Tip Resistance and Crack Closure Phenomena," in Progress in Flaw Growth and Fracture Toughness Testing, ASTM STP 536, American Society for Testing and Materials, pp. 5-21, 1973.

8.   Pitoniak, F.J., Grandt, A.F., Montulli, L.T., and Packman, P.F., "Fatigue Crack Retardation and Closure in Polymethylmethacrylate," Engineering Fracture Mechanics, 6, 663 (1974).

9.   Barton, J.R., "Quantitative Correlation Between Magnetic Perturbation Signatures and Inclusions," in Bearing Steels: The Rating of Nonmetallic Inclusions, ASTM STP 575, American Society for Testing and Materials, pp. 189-213, 1975.

10.   Bathias, C., and Pelloux, R.M., "Fatigue Crack Propagation in Martensitic and Stainless Steels," Met. Trans. 4, 1265 (1973).

11.   Lankford, J., Davidson, D.L., and Cook, T.S., "Fatigue Crack Tip Plasticity," in Cyclic Stress-Strain and Plastic Deformation, ASTM STP 637, American Society for Testing and Materials, pp. 37-53, 1977.

12.   Ko, W.L., and Francis, P.H., "Magnetic Field Leakage Due to a Surface Crack," Brit. J. of Nondest. Test. 17, No. 5, 141 (1975).

13.   Francis, P.H. and Davidson, D.L., "Experimental Characterization of Yield Induced by Surface Flaws," in The Surface Crack: Physical Problems and Computational Solutions, ASME Publication H29, pp. 63-78, 1972.

14.   Francis, P.H., Davidson, D.L., and Forman, R.G., "An Experimental Investigation into the Mechanics of Deep Semi-Elliptical Surface Cracks in Mode I Loading," Eng. Fract. Mech. 4, 617 (1972).

APPENDIX A

ERRATA TO INTERIM SCIENTIFIC REPORT
AFOSR-TR-77-0191

NONDESTRUCTIVE EVALUATION OF METAL FATIGUE
Interim Scientific Report, AFOSR-TR-77-0191 Contract F44620-75-C-0042
February 1977

ERRATA

In all of the locations listed below, change "AF 1410" to "HY 180"

Page No.	Paragraph	Line No.
Form 1473	Abstract	18
Abstract		17
Table of Contents	Section II. B.	
1	1	14
6	6	6
7	Heading, Section B	
7	1	1
7	2	1
22	i	2
22	1	12

APPENDIX B

MAGNETIC PERTURBATION, ULTRASONIC SURFACE WAVE,
BARKHAUSEN NOISE ANALYSIS, ELECTRIC CURRENT
INJECTION, AND AC FOUR-CONTACT ELECTRIC
PROBE TECHNIQUES

1.   Magnetic Perturbation

In the magnetic perturbation method, an electromagnet is used to magnetize the specimen while the surface of the specimen is scanned with a small magnetometer to detect minute perturbations in the magnetic leakage field. Perturbations can be caused by defects in the specimen such as inclusions, voids, cracks, localized residual stresses, chemical segregation, etc. The method is schematically illustrated in Figure B-1 for the case of an inclusion. In the present program, magnetic perturbation inspection of the specimen was accomplished by scanning the surface of the specimen with a Hall-effect transducer that transforms the magnetic perturbations into electrical signals which are then recorded. Recent improvements in Hall probe design have made it possible to resolve heretofore unobservable changes in magnetic signal characteristics associated with fatigue crack development in the vicinity of tiny material inclusions. The magnetic perturbation method is particularly applicable to fatigue evaluation studies because it is sensitive not only to actual discontinuities but also to local stresses and/or strains associated with developing fatigue cracks.

2.   Ultrasonic Surface Waves

In the ultrasonic surface wave method, wedge-shaped transducers attached to the specimen are used to propagate pulses of acoustical energy as surface waves along the specimen surfaces. As the propagating pulse of surface wave energy encounters a defect, such as a crack with separated interfaces, a portion of the energy is reflected back towards the transducer, as illustrated schematically in Figure B-2, where it is received and displayed on an oscilloscope trace as a signal or "echo". When using this "pulse echo" method to monitor a specimen during stress cycling, if an "echo" or signal which was not present initially appears on the oscilloscope trace, it is an indication that a fatigue crack has developed. It has been substantiated in previous work, that the fatigue crack must have separated interfaces, that is, it must be "open", in order for sufficient acoustic energy to be reflected to make the crack detectable. The ultrasonic surface wave technique has excellent resolution for surface fatigue cracks in both ferromagnetic and nonferromagnetic metals and can be used to continuously monitor specimens during stress cycling.

3.   Barkhausen Noise Analysis

The Barkhausen noise analysis method involves applications of a controlled magnetic field sequence to the specimen which causes a rearrangement of the magnetic domain structure. The domain rearrangements occur abruptly and the associated discrete changes in specimen magnetization induce voltage pulses in a detection coil placed in proximity to the specimen. This

approach is illustrated schematically in Figure B-3. The Barkhausen noise
is strongly influenced by various parameters of the specimen, in particular
the state of mechanical stress, and therefore it can be used to determine
the residual stress around a fatigue crack. In experiments performed on
fatigue specimens mounted in the Fatigue Testing Machine, the controlled
magnetic field sequence was applied with the same magnetizing coil used
for the magnetic perturbation experiments. The Barkhausen probe was a
small inductive coil which could be mounted on a micrometer adjustment
fixture.

4.   Electric Current Injection

The electric current injection method for investigating fatigue cracks
in nonferromagnetic metals is analogous to the magnetic perturbation method
used for magnetic materials. Figure B-4 is a schematic illustration of the
method. A specimen is inspected utilizing this method by establishing a
suitable current flow in the specimen and detecting deviations in this current
flow caused by material inhomogeneities, such as inclusions, chemical
segregations, cracks, etc. The deviations in current flow produce pertur-
bances in the associated magnetic field and these are detected by a small
noncontacting magnetometer probe scanned over the specimen surface.
The signal output information from the probe is an electrical voltage and
can be readily displayed on an oscilloscope or printed out on a strip chart
recorder.

5.   AC Four-Contact Electric Probe

The AC four-contact electric probe method is an electrical potential
approach whereby two outer electrical contacts inject current and two inner
contacts sense the electric potential, as shown schematically in Figure B-5a.
The presence of a crack between the inner contacts causes a disruption of
the electric potential due to the insulating barrier formed by the crack, as
shown in Figure B-5b. By comparing the voltages measured at constant
current on cracked and uncracked specimens, in principle, electric potential
theory can be used to precisely calculate the crack depth. In practice,
however, it has been found more convenient to calibrate the probe using a
reference flaw, i.e., a machined slot which simulates the anticipated crack
size, shape and location. The AC approach circumvents the difficulties
associated with the generation of thermal emf's. encountered in the conven-
tional DC approach. Adequate penetration depth is obtained with the AC
method by using low frequency (100 Hz), and synchronous detection is used
to discriminate against incoherent noise, resulting in much greater sensi-
tivity than can be obtained with the DC technique. This greater sensitivity
permits the use of very small drive currents, on the order of 16 ma.
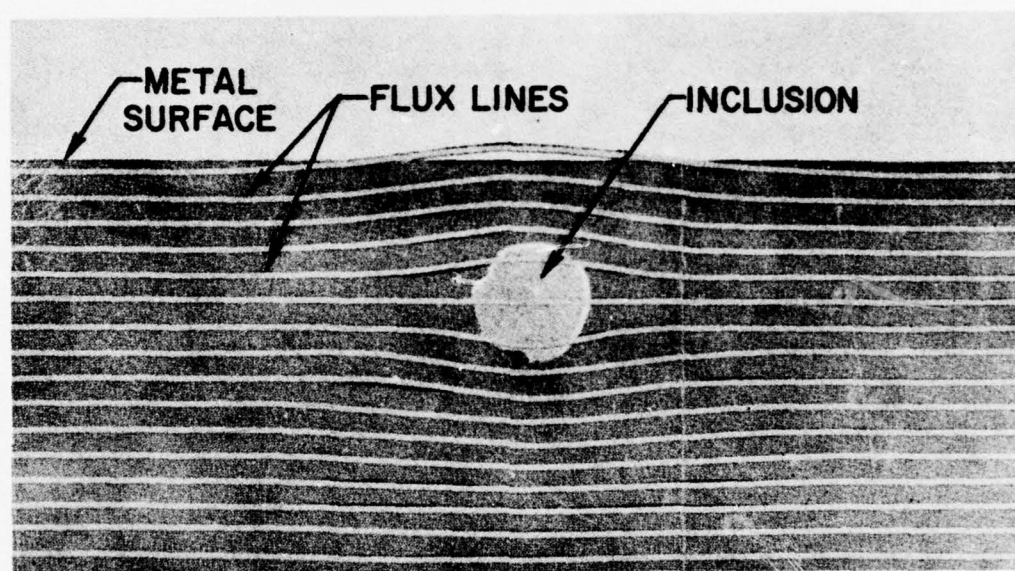
1155

FIGURE B-1. PERTURBATIONS IN MAGNETIC FLUX CAUSED BY
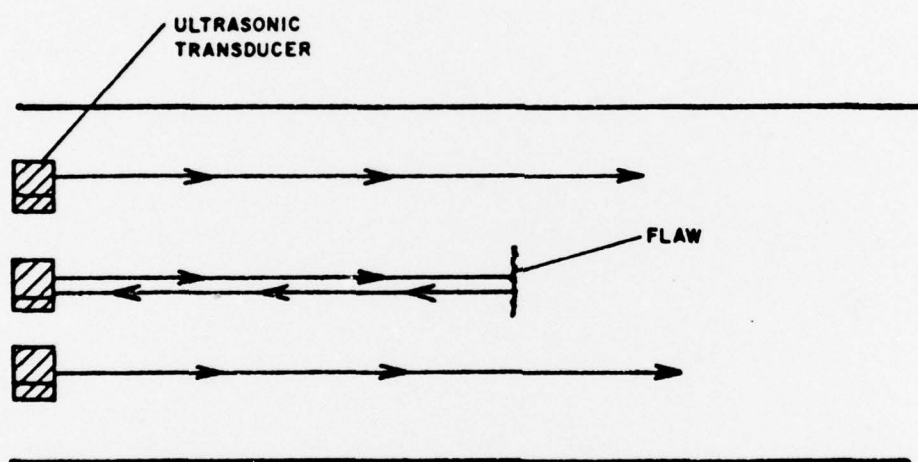INCLUSION IN FERROMAGNETIC MATERIAL

FIGURE B-2 ULTRASONIC SURFACE WAVE PULSE-ECHO
METHOD. Influence of a Flaw on Propagation
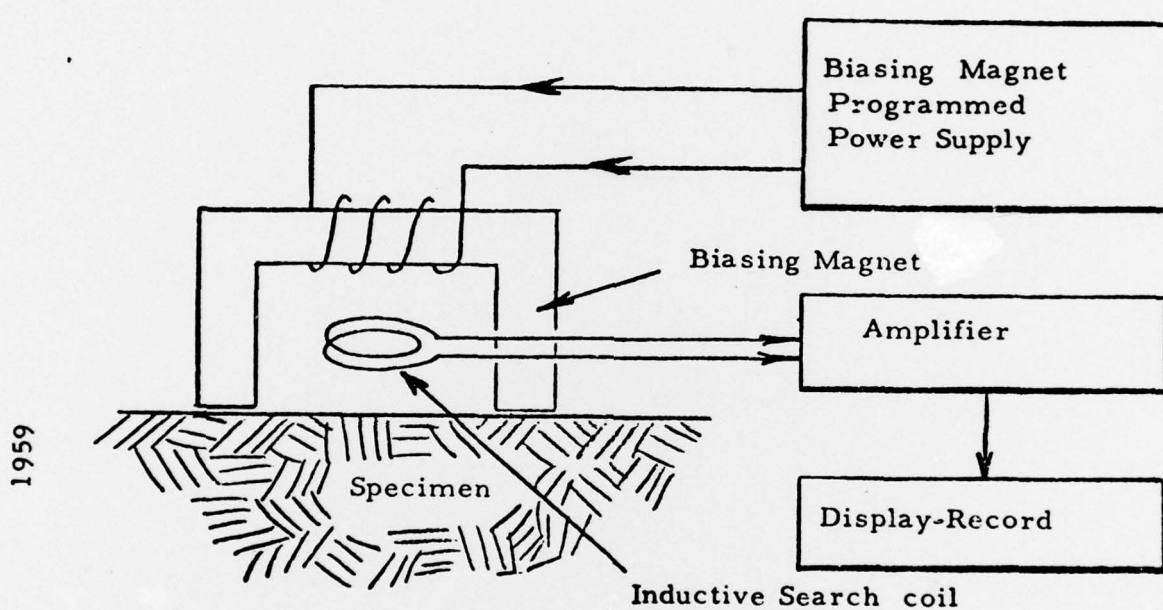of Acoustic Energy.

1959

FIGURE B-3 SCHEMATIC DIAGRAM OF THE ESSENTIAL FEATURES
OF AN ARRANGEMENT FOR INDUCTIVELY SENSING THE
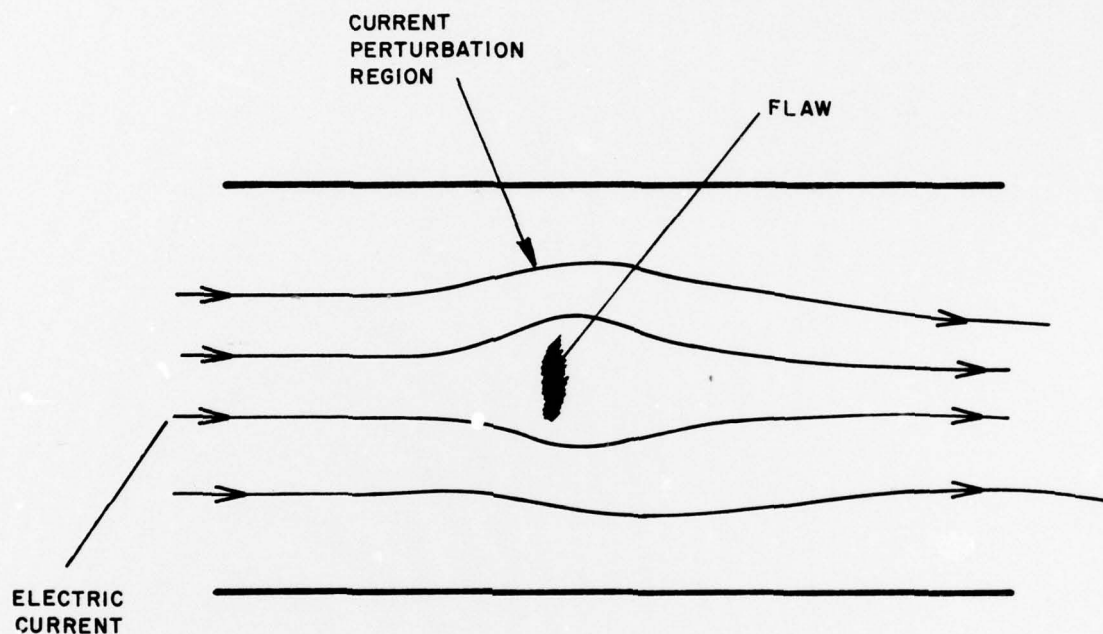BARKHAUSEN EFFECT

1641

FIGURE B-4. ELECTRIC CURRENT INJECTION METHOD
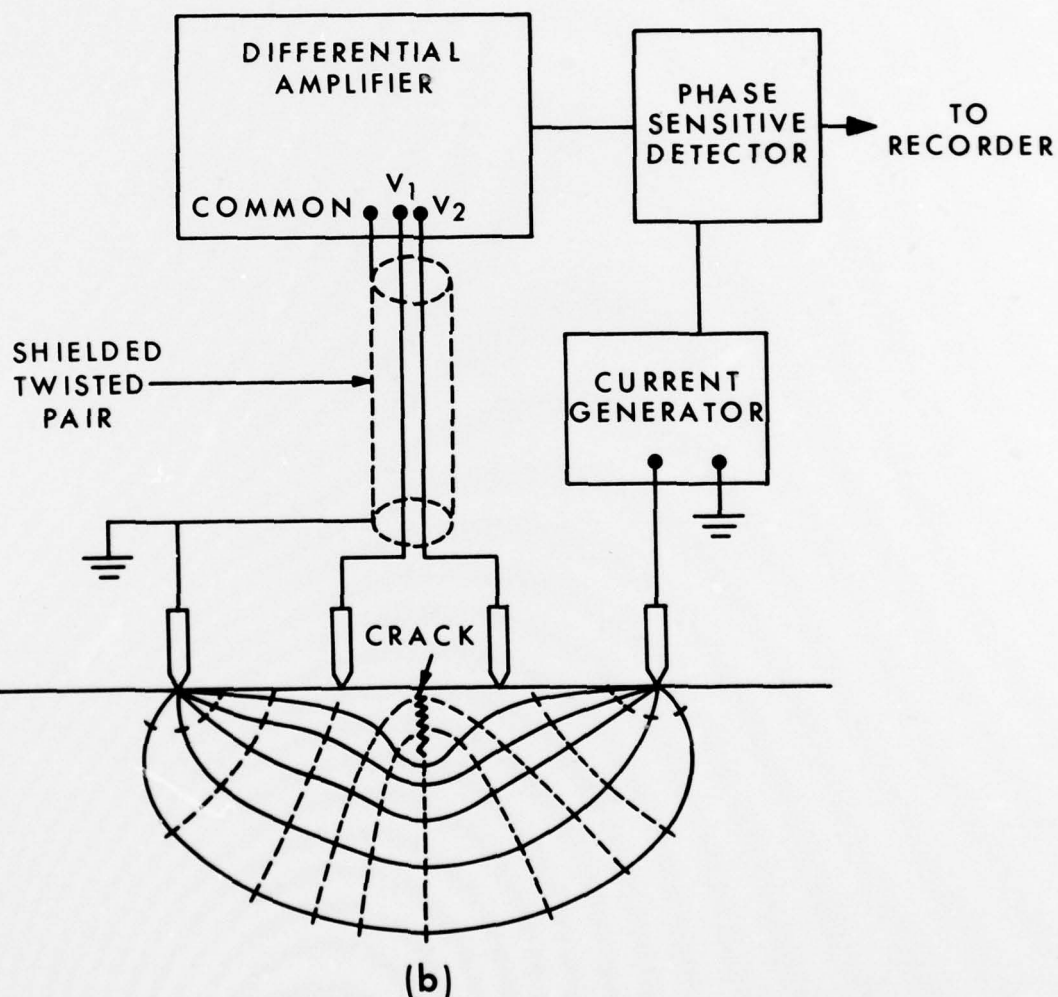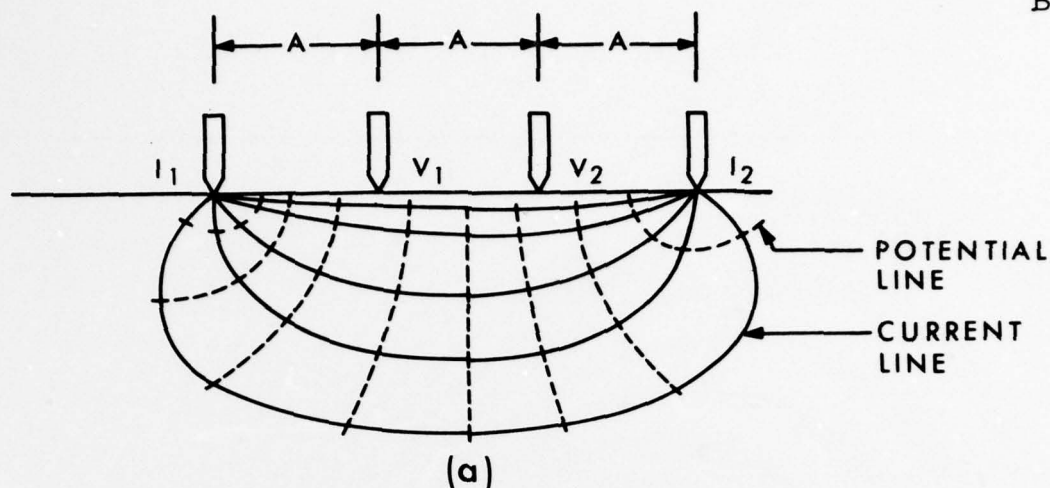Influence of a Flaw on Electric Current
Distribution

FIGURE B-5. OPERATION OF AC FOUR CONTACT ELECTRIC PROBE
(a) ON UNCRACKED AND (b) ON CRACKED MATERIAL. The
current contacts I_1 and I_D are driven by a current generator.
The signal from the voltage contacts V_1 and V_2 is amplified
and synchronously detected.

APPENDIX C

ROD-TYPE FATIGUE SPECIMEN PREPARATION
AND MATERIAL PROPERTIES

1.   AISI 4340 Steel Specimens

Tensile fatigue specimens of AISI 4340 steel were rough-machined
to shape from one-inch diameter bar stock which had been austenitized at
1525°F for two hours, oil-quenched, and air tempered for four hours at
975°F. Hardness readings resulting from this heat treatment were in the
range 35-37 Rc. Final machining (grinding) and polishing operations
followed. All specimens were hand polished using successively finer
carborundum and emergy papers, ending with No. 4/0, followed by final
polishing with 0.3-μ alumia. The specimen configuration is shown in
Figure C-1.

The average mechanical properties of the specimen materials
obtained from specimen tests are summarized in Table C-1.

TABLE C-1

AVERAGE MECHANICAL PROPERTIES OF
AISI 4340 SPECIMEN MATERIAL

Ultimate tensile strength	194,000 ksi
0. 2% tensile yield strength	183,000 ksi
Elastic modulus	35×10^6 psi
% elongation at fracture	14.3
% reduction in area at fracture	48.5

2.   HY 180 Steel Specimens

Tensile fatigue specimens of HY 180 steel were rough-machined
to shape from 1.7-inch thick plate stock obtained from General Dynamics
Convair Aerospace Division in Fort Worth, Texas. The heat number
indicated on the material was HT C52200. Heat treatment, putting the
plate material into the solution-treated and aged condition had been per-
formed by U. S. Steel according to the following schedule:

Initial austenizing	1650°F for 60 minutes
Final austenizing	1500°F for 60 minutes
Aging	950°F for 8 hours

The material was water quenched after each heat treatment. Composition
in weight percent as given by U. S. Steel is:

C	0.12	S	0.003
Mn	0.13	Si	0.07
P	0.007	Ni	9.93
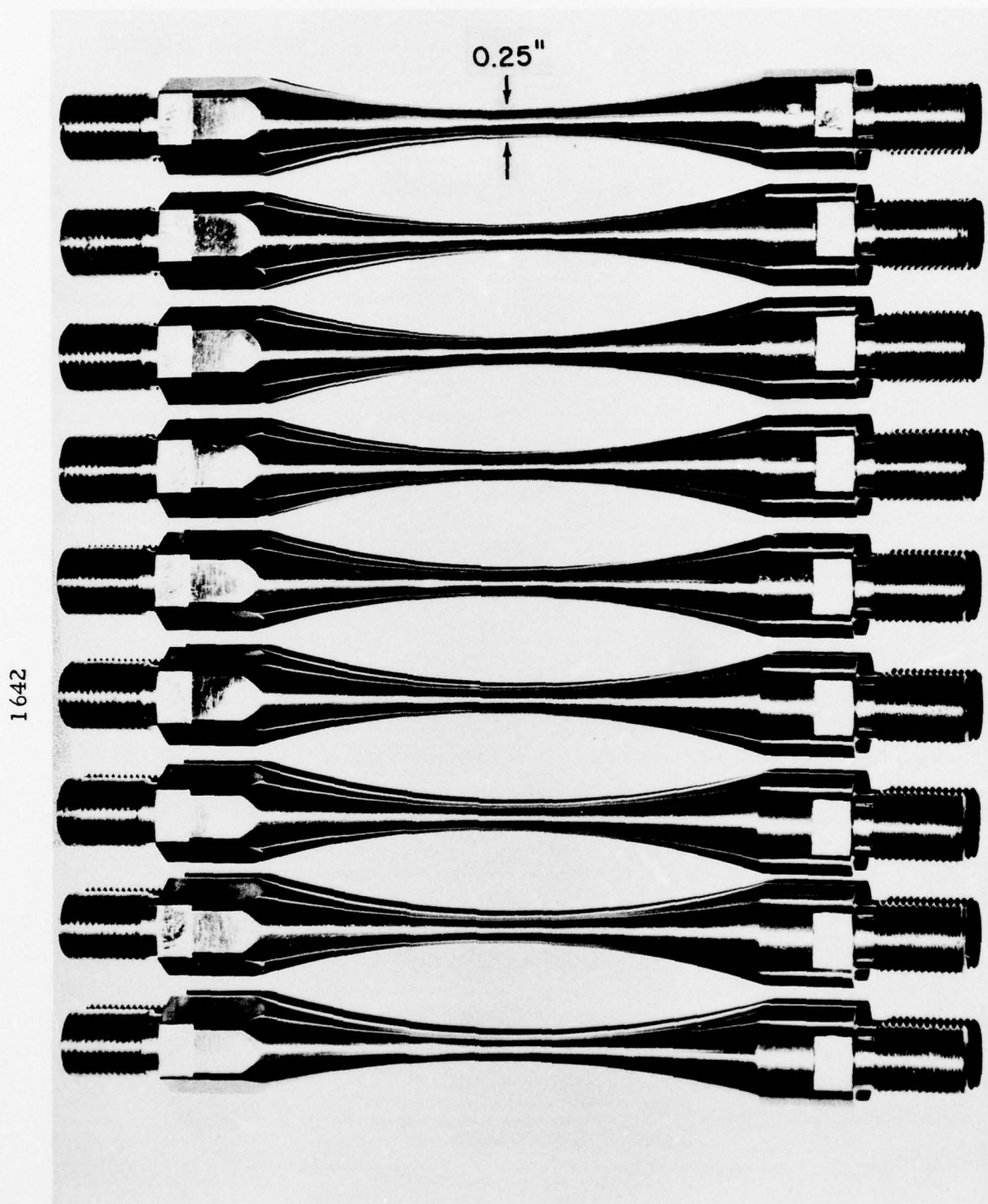
FIGURE C-1.   PHOTOGRAPH SHOWING SEVERAL TYPICAL AISI 4340
STEEL TEST SPECIMENS

Cr	2.00	Al	0.017
Mo	0.99	N	75 PPM
Co	7.76	O	25 PPM
Ti	0.01		

Hardness readings made at SwRI on the machined fatigue specimens prior to finish grinding indicated a Rockwell hardness of approximately 43 Rc. Final grinding and polishing operations were performed in a manner similar to the AISI 4340 specimens.

The average mechanical properties as reported by General Dynamics for plate specimens are summarized in Table C-II.

TABLE C-II

AVERAGE MECHANICAL PROPERTIES OF HY 180 SPECIMEN MATERIAL

Ultimate tensile strength	196,000 psi
0.2% tensile yield strength	183,000 psi
% elongation	18.0
% reduction in area	73.8

3. Tabulation of Fatigue Specimens

A tabulation of the fatigue specimens used in this program is given in Table C-III.

TABLE C-III

SUMMARY OF SPECIMEN INFORMATION

Specimen No.	Material	Peak[1] Stress at Specimen Center (ksi)	Number of Cycles[2] (millions)	Final Crack Length (in.)	ΔL[3] (in.)	Type	Tracks Other than Crack Center	Expanded Traces	Ultrasonic Inspection	Barkhausen Inspection	Electric Current Injection	Four-Contact Electric Probe	Remarks
						Initiation of Crack	Magnetic Perturbation Inspection						
S5	AISI 4340	180	0.0024	0.048 / 0.052	-0.045 / -0.040	Surface Inclusion	Yes	Yes	Yes	Yes	No	No	Two Cracks Fractography
S29	AISI 4340	130	0.0956	0.050	+0.010	Surface Inclusion	Yes	No	Yes	No	No	No	
S30	AISI 4340	130	0.1102	0.050	+0.010	Surface Inclusion	Yes	No	Yes	Yes	No	No	Microhardness
H1	HY 180	180	0.8476	0.052	-0.040	Surface Pore	Yes	Yes	Yes	Yes	No	No	Fractography
T1	Ti-6Al-4V	120	0.0386	0.051	-0.110	Undetermined	No	No	Yes	No	No	Yes	

NOTES: (1) Maximum tensile stress at midpoint of specimen length, mean stress equal 0.5 maximum.
(2) Total number of stress cycles.
(3) Location of failure initiation or crack relative to midpoint of specimen length.